Droplets Generation Mechanisms by Graphite Cathodes in the Vacuum Arc Deposition Technique

BY

MUNTHER KANDAH

DEPARTMENT OF CHEMICAL ENGINEERING

McGILL UNIVERSITY, MONTREAL

JUNE 1993

A THESIS SUBMITTED TO THE FACULTY OF GRADUATE STUDIES AND RESEARCH IN PARTIAL FULFILMENT OF THE REQUIREMENTS OF THE DEGREE OF MASTER IN ENGINEERING

Munther Kandah, 1993

Name GUNTHER ISSA KANDAH

Dissertation Abstracts International is arranged by broad, general subject categories. Please select the one subject which most nearly describes the content of your dissertation. Enter the corresponding four-digit code in the spaces provided.

Fluid and Plasma
SUBJECT TERM

0 7 5 9
SUBJECT CODE

U·M·I

Subject Categories

THE HUMANITIES AND SOCIAL SCIENCES

COMMUNICATIONS AND THE ARTS

Architecture	0729
Art History	0377
Cinema	0900
Dance	0378
Fine Arts	0357
Information Science	0723
Journalism	0391
Library Science	0399
Mass Communications	0708
Music	0413
Speech Communication	0459
Theater	0465

EDUCATION

General	0515
Administration	0514
Adult and Continuing	0516
Agricultural	0517
Art	0273
Bilingual and Multicultural	0282
Business	0688
Community College	0275
Curriculum and Instruction	0727
Early Childhood	0518
Elementary	0524
Finance	0277
Guidance and Counseling	0519
Health	0680
Higher	0745
History of	0520
Home Economics	0278
Industrial	0521
Language and Literature	0279
Mathematics	0280
Music	0522
Philosophy of	0998
Physical	0523
Psychology	0525
Reading	0535
Religious	0527
Sciences	0714
Secondary	0533
Social Sciences	0534
Sociology of	0340
Special	0529
Teacher Training	0530
Technology	0710
Tests and Measurements	0288
Vocational	0747

LANGUAGE, LITERATURE AND LINGUISTICS

Language	
General	0679
Ancient	0289
Linguistics	0290
Modern	0291
Literature	
General	0401
Classical	0294
Comparative	0295
Medieval	0297
Modern	0298
African	0316
American	0591
Asian	0305
Canadian (English)	0352
Canadian (French)	0355
English	0593
Germanic	0311
Latin American	0312
Middle Eastern	0315
Romance	0313
Slavic and East European	0314

PHILOSOPHY, RELIGION AND THEOLOGY

Philosophy	0422
Religion	
General	0318
Biblical Studies	0321
Clergy	0319
History of	0320
Philosophy of	0322
Theology	0469

SOCIAL SCIENCES

American Studies	0323
Anthropology	
Archaeology	0324
Cultural	0326
Physical	0327
Business Administration	
General	0310
Accounting	0272
Banking	0770
Management	0454
Marketing	0338
Canadian Studies	0385
Economics	
General	0501
Agricultural	0503
Commerce Business	0505
Finance	0508
History	0509
Labor	0510
Theory	0511
Folklore	0358
Geography	0366
Gerontology	0351
History	
General	0578
Ancient	0579
Medieval	0581
Modern	0582
Black	0328
African	0331
Asia, Australia and Oceania	0332
Canadian	0334
European	0335
Latin American	0336
Middle Eastern	0333
United States	0337
History of Science	0585
Law	0398
Political Science	
General	0615
International Law and Relations	0616
Public Administration	0617
Recreation	0814
Social Work	0452
Sociology	
General	0626
Criminology and Penology	0627
Demography	0938
Ethnic and Racial Studies	0631
Individual and Family Studies	0628
Industrial and Labor Relations	0629
Public and Social Welfare	0630
Social Structure and Development	0700
Theory and Methods	0344
Transportation	0709
Urban and Regional Planning	0999
Women's Studies	0453

THE SCIENCES AND ENGINEERING

BIOLOGICAL SCIENCES

Agriculture	
General	0473
Agronomy	0285
Animal Culture and Nutrition	0475
Animal Pathology	0476
Food Science and Technology	0359
Forestry and Wildlife	0478
Plant Culture	0479
Plant Pathology	0480
Plant Physiology	0817
Range Management	0777
Wood Technology	0746
Biology	
General	0306
Anatomy	0287
Biostatistics	0308
Botany	0309
Cell	0379
Ecology	0329
Entomology	0353
Genetics	0369
Limnology	0793
Microbiology	0410
Molecular	0307
Neuroscience	0317
Oceanography	0416
Physiology	0433
Radiation	0821
Veterinary Science	0778
Zoology	0472
Biophysics	
General	0786
Medical	0760

EARTH SCIENCES

Biogeochemistry	0425
Geochemistry	0996
Geodesy	0370
Geology	0372
Geophysics	0373
Hydrology	0388
Mineralogy	0411
Paleobotany	0345
Paleoecology	0426
Paleontology	0418
Paleozoology	0985
Palynology	0427
Physical Geography	0368
Physical Oceanography	0415

HEALTH AND ENVIRONMENTAL SCIENCES

Environmental Sciences	0768
Health Sciences	
General	0566
Audiology	0300
Chemotherapy	0992
Dentistry	0567
Education	0350
Hospital Management	0769
Human Development	0758
Immunology	0982
Medicine and Surgery	0564
Mental Health	0347
Nursing	0569
Nutrition	0570
Obstetrics and Gynecology	0380
Occupational Health and Therapy	0354
Ophthalmology	0381
Pathology	0571
Pharmacology	0419
Pharmacy	0572
Physical Therapy	0382
Public Health	0573
Radiology	0574
Recreation	0575
Speech Pathology	0460
Toxicology	0383
Home Economics	0386

PHYSICAL SCIENCES

Pure Sciences

Chemistry	
General	0485
Agricultural	0749
Analytical	0486
Biochemistry	0487
Inorganic	0488
Nuclear	0738
Organic	0490
Pharmaceutical	0491
Physical	0494
Polymer	0495
Radiation	0754
Mathematics	0405
Physics	
General	0605
Acoustics	0986
Astronomy and Astrophysics	0606
Atmospheric Science	0608
Atomic	0748
Electronics and Electricity	0607
Elementary Particles and High Energy	0798
Fluid and Plasma	0759
Molecular	0609
Nuclear	0610
Optics	0752
Radiation	0756
Solid State	0611
Statistics	0463

Applied Sciences

Applied Mechanics	0346
Computer Science	0984
Engineering	
General	0537
Aerospace	0538
Agricultural	0539
Automotive	0540
Biomedical	0541
Chemical	0542
Civil	0543
Electronics and Electrical	0544
Heat and Thermodynamics	0348
Hydraulic	0545
Industrial	0546
Marine	0547
Materials Science	0794
Mechanical	0548
Metallurgy	0743
Mining	0551
Nuclear	0552
Packaging	0549
Petroleum	0765
Sanitary and Municipal	0554
System Science	0790
Geotechnology	0428
Operations Research	0796
Plastics Technology	0795
Textile Technology	0994

PSYCHOLOGY

General	0621
Behavioral	0384
Clinical	0622
Developmental	0620
Experimental	0623
Industrial	0624
Personality	0625
Physiological	0989
Psychobiology	0349
Psychometrics	0632
Social	0451

Droplets Generation Mechanisms by Graphite in Vacuum Arc Deposition

LIST OF TABLES

LIST OF FIGURES

ACKNOWLEDGMENT

ABSTRACT

INTRODUCTION 1

1-1 : VACUUM ARC DEPOSITION

1-1-1 : WHAT IS VAD ? 3

1-1-2 : BASIC VAD SYSTEM 6

1-1-3 : SOME CHARACTERISTICS FEATURES OF VAD 8

1-1-4 : VACUUM ARCS ON CARBON CATHODES 11

1-2 : DROPLETS

1-2-1 : LITERATURE REVIEW ON DROPLETS 16

1-2-2 : PREVIOUS WORK ON VAD CARBON FILMS AT McGILL 20

1-3 : CARBON

1-3-1 : DIAMOND AND DIAMOND-LIKE CARBON 27

1-3-2 : APPLICATION OF DIAMOND-LIKE FILMS 30

1-4 : OBJECTIVES 31

2-1 : EXPERIMENTAL SET-UP

- CO_2-TEA LASER 32

- ELECTRICAL CIRCUIT 33

- CURRENT MEASUREMENT 36

- ELECTRODES 38

- SUBSTRATE 40

- PUMPING SYSTEM 41

2-2 : EXPERIMENTAL PROCEDURE

2-2-1 : DEPOSITION EXPERIMENT 42

2-2-2 : TEMPERATURE DISTRIBUTION 43

2-2-3 : COOLING TEMPERATURE CURVE 48

2-2-4 : PARTICLE DIAGNOSTICS 54

3-1 : EXPERIMENTAL RESULTS 56

3-1-1 : NUMBER AND SIZE OF PARTICLES

- ARC CURRENT LEVEL 58

- DISTANCE BETWEEN THE CATHODE AND THE SUBSTRATE 62

- ARC TIME 67

-CATHODE SPOT TEMPERATURE 70

3-1-2 : ORIGIN OF PARTICLES 79

3-1-3 : PARTICLES STRUCTURE 83

DISCUSSION 91

CONCLUSION 97

REFERENCES

LIST OF TABLES

TABLE(1-1): BASIC CHARACTERISTICS OF a-C:H.

TABLE(1-2): APPLICATIONS OF DIAMOND-LIKE FILMS.

TABLE(3-1): OPERATING CONDITIONS.

LIST OF FIGURES

FIGURE(1-1): VACUUM ARC DEPOSITION SYSTEM.

FIGURE(1-2): CATHODE SPOT REGION OF A VACUUM ARC.

FIGURE(1-3): A BASIC VAD COATING SYSTEM.

FIGURE(1-4): SCHEMATIC REPRESENTATION OF COATING APPARATUSES WITH DIFFERENT GEOMETRIES.

FIGURE(1-5): DISTRIBUTION OF POTENTIAL AS A FUNCTION OF POSITION BETWEEN TWO CONDUCTING BOUNDARIES ENCLOSING A PLASMA VOLUME.

FIGURE(1-6): DC-VOLT-AMPERE CHARACTERISTICS OF VACUUM ARCS.

FIGURE(1-7): RESULTS FOR THE MOST PROBABLE VALUES OF ARC ION ENERGY DIVIDED BY ION CHARGES AS A FUNCTION OF CURRENT FOR SINGLY AND DOUBLY IONIZED CATHODE IONS.

FIGURE(1-8): ANGULAR DISTRIBUTION OF PARTICLE MASS EMISSION IN A VACUUM ARC ON A 25-mm DIAMETER COPPER CATHODE.

FIGURE(1-9): a) SEM RECORDING OF A DEPOSIT MADE ON TUNGSTEN IN VACUUM($P=10^{-2}$ Pa) WITH T=470 C & Vs=-300V

b) CLOSE-UP OF (a) SHOWING THE STRUCTURE OF SPHERES IMBEDDED IN DEPOSIT.

FIGURE(1-10): AES SPECTRUM OF A DEPOSIT MADE ON TUNGSTEN IN VACUUM ($P=10^{-2}$ Pa) WITH T=470 C AND Vs=-900 V.

FIGURE(1-11): RAMAN SPECTRUM OF A DEPOSIT MADE ON NICKEL IN VACUUM ($P=10^{-2}$ Pa) WITH T=470 C & Vs=0 V.

FIGURE(2-1a): GEOMETRY OF ELECTRODES AND TRIGGERING ARRANGEMENT.

FIGURE(2-1b): VACUUM CHAMBER AND PUMPING ARRANGEMENT.

FIGURE(2-2) : SIGNALS PRODUCED FROM SHUNT AND PEARSON CURRENT TRANSFORMER.

FIGURE(2-3) : GRAPHITE CATHODE AND GRAPHITE ANODE.

FIGURE(2-4) : a) SCHEMATIC FOR THE HEATED VOLUME ON THE CATHODE SURFACE.

b) EFFECT OF CONDUCTIVITY THROUGH THE CATHODE.

FIGURE(2-5) : CATHODE SPOT TEMPERATURE AS A FUNCTION OF ARC TIME FOR I= 110 A, 77.5 A & 44 A CALCULATED FROM EQ. 2-5.

FIGURE(2-6) : SCHEMATIC DISTRIBUTION OF THE TEMPERATURE.

FIGURE(2-7) : VALUES OF THE DIMENSIONLESS FUNCTION ($f_2=x^2/\alpha t$).

FIGURE(2-8) : COOLING TEMPERATURE OF CATHODE SPOT AS A FUNCTION OF TIME FOR I= 44 A, AT X=0.

FIGURE(2-9) : COOLING TEMPERATURE OF CATHODE SPOT AS A FUNCTION OF TIME FOR I= 77.5 A, AT X=0.

FIGURE(2-10): COOLING TEMPERATURE OF CATHODE SPOT AS A FUNCTION OF TIME FOR I= 110 A, AT X=0.

FIGURE(3-1): NUMBER DENSITY OF PARTICLES AS A FUNCTION OF ELECTRIC CHARGE THROUGH CATHODE FOR I=44 AND 110 A, D= 75 mm, t=14 ms.

FIGURE(3-2): NUMBER DENSITY OF PARTICLES AS A FUNCTION OF ELECTRIC CHARGE THROUGH CATHODE FOR I=44 AND 110 A, D=130 mm, t=14 ms.

FIGURE(3-3): NUMBER DENSITY OF PARTICLES AS A FUNCTION OF ELECTRIC CHARGE THROUGH CATHODE FOR TWO DISTANCES BETWEEN CATHODE AND SUBSTRATE, FOR I=44 A AND t=14 ms.

FIGURE(3-4): NUMBER DENSITY OF PARTICLES AS A FUNCTION OF ELECTRIC CHARGE THROUGH CATHODE FOR TWO DISTANCES BETWEEN CATHODE AND SUBSTRATE, FOR I=110 A AND t=14 ms.

FIGURE(3-5): DATA OF FIGURE (3-3) AND (3-4) NORMALIZED TO THE SOLID ANGLE OF THE SUBSTRATE AS VIEWED BY THE CATHODE.

FIGURE(3-6): NUMBER DENSITY OF PARTICLES AS A FUNCTION OF THE ARC DURATION TIME ,FOR I= 44, 77.5, AND 110 A, AT D=75 mm.

FIGURE(3-7): NUMBER DENSITY OF PARTICLES AS A FUNCTION OF CALCULATED CATHODE SPOT TEMPERATURE FROM EQ. 2-5.

FIGURE(3-8a): PARTICLE SIZE DISTRIBUTION FOR CATHODE SPOT TEMPERATURE AROUND 700 K, CALCULATED FROM EQ.2-5.

FIGURE(3-8b): PARTICLE SIZE DISTRIBUTION FOR CATHODE SPOT TEMPERATURE AROUND 1902 K,CALCULATED FROM EQ.2-5.

FIGURE(3-8c): PARTICLE SIZE DISTRIBUTION FOR CATHODE SPOT TEMPERATURE AROUND 3059 K,CALCULATED FROM EQ.2-5.

FIGURE(3-8d): PARTICLE SIZE DISTRIBUTION FOR CATHODE SPOT TEMPERATURE AROUND 5538 K,CALCULATED FROM EQ.2-5.

FIGURE(3-9) : SEM RECORDING OF A DEPOSIT ON SILICON IN VACUUM $P=10^{-4}$ TORR, AND t=5 ms, SHOWING A LARGE PARTICLE DISSOCIATED INTO SEVERAL SMALL PARTICLES ON IMPACT.

FIGURE(3-10): SEM RECORDING OF A DEPOSIT ON SILICON IN VACUUM ($P=10^{-4}$ TORR), AND COMPLETE DISCHARGE, SHOWING SMALL PARTICLES AGGLOMERATED TO FORM LARGE PARTICLES.

FIGURE(3-11): PHOTOGRAPH SHOWING THE EMISSION OF THE PARTICLES FROM THE CATHODE TO THE SUBSTRATE.

FIGURE(3-12): PHOTOGRAPH SHOWING THE EMISSION OF THE PARTICLES FROM THE ANODE, AND REFLECTED FAR FROM THE SUBSTRATE.

FIGURE(3-13): TYPICAL AES SPECTRA FOR DIAMOND, GRAPHITE, AND AMORPHOUS CARBON FILM.

FIGURE(3-14): AES SPECTRUM FOR A PARTICLE DEPOSITED ON SILICON IN VACUUM $P=10^{-4}$ TORR, t=14 ms, D=7.5 cm, AND Q=100 C.

FIGURE(3-15): AES SPECTRUM FOR ANOTHER PARTICLE ON THE SAME SAMPLE SHOWN IN FIGURE (3-14).

FIGURE(3-16): AES SPECTRUM FOR THE BACKGROUND DEPOSITED ON SILICON IN VACUUM P=10^{-4} TORR, t=14 ms, D=7.5 cm, AND Q=100 C.

FIGURE(3-17): AES SPECTRUM FOR THE BACKGROUND DEPOSITED ON SILICON IN VACUUM P=10^{-4} TORR, t=14 ms, D=45 cm, AND Q= 100 C.

FIGURE(3-18): SEM RECORDING SHOWING THE MORPHOLOGY OF A DEPOSITION ON SILICON IN VACUUM P=10^{-4} TORR, t=14 ms, D=45 cm, AND Q=100 C.

FIGURE(3-19): SEM RECORDING SHOWING THE MORPHOLOGY OF A DEPOSIT ON SILICON IN VACUUM P=10^{-4} TORR, t=14 ms, D=7.5 cm, AND Q= 100 C.

FIGURE(3-20): AES SPECTRUM FOR A PARTICLE DEPOSITED ON SILICON IN VACUUM P=10^{-4} TORR, t=0.5 ms, D=7.5 cm, AND Q=100 C.

ACKNOWLEDGMENT

The support of the Jordan University of Science and Technology for sponsoring this research is gratefully acknowledged.

I am grateful to Mrs H. Campbell from the metallurgical Engineering Department for her help in using SEM & Image Analyzer Software. I would like to thank Mr Alain Joly from IREQ for his help using AES. The author is also grateful to Mr Jean Dumont, who is always ready to help all the graduate students by preparing any thing needed for their research, and also many thanks for all the technical staff working in the Chemical Engineering Workshop, and to Mr L. Cusmich from the electronic workshop.

I would like to say thank you very very much Dr Jean-Luc Meunier, for your great help during the setting up of the experiment and for your valuable comments on the results.

RESUME

Le problème le plus important dans la technique de déposition par arc dans le vide est la formation de particules de l'ordre du micron dans les films. Ces particules induisent une dégradation des propriétés du revêtement. La présente étude est reliée aux mécanismes de génération de ces particules et aux caractéristiques des gouttelettes produites dans les couches de carbone déposées par arc dans le vide. Dans le but de mieux contrôler les mécanismes de génération de ces particules, les effets du courant d'arc, de la durée de l'arc, de la température au niveau des spots cathodiques et de la distance entre la cathode et le substrat sur la grosseur et la quantité des particules sont étudiés.

Les particules observées dans les dépôts ont des diamètres variant de 0.3 μm à 2 μm avec une structure graphitique. Leur grandeur et le nombre de ces particules est proportionnel à la température du spot cathodique (i.e. au courant d'arc et/ou sa durée), et inversement proportionnel à la distance entre la cathode et le substrat. La production de gouttelettes est essentiellement due aux effets de chauffage au niveau de la cathode.

ABSTRACT

The most severe problem for the vacuum arc deposition (VAD) technique is the formation of micron-size particles on the films. These particles degrade the films properties. The present work studied the generation mechanisms and characteristics of the droplets that are produced in the carbon films deposited by vacuum arc technique. To achieve a better control of the generation mechanism of these droplets, the effect of the arc current, arc duration time, cathode spot temperature and distance between cathode and substrate on the size and population of the micro-droplets are studied.

The micro-droplets are in the range of 0.3 μm to 2 μm in diameter, and have a graphite structure. The most probable origin for these particles are the cathode. The size and population of these particles are directly proportional to the cathode spot temperature (i.e., to the arc current and/or arc duration time), and inversely proportional to the distance between the cathode and the substrate. The droplet production is mainly due to the heating effect.

INTRODUCTION

Vacuum arc is a paradox, because, if there is a vacuum there is no arc, and if there is an arc there is no vacuum. The term vacuum arc, as employed here, means an arc sustained by material originating from cathode in an environment that would otherwise be a vacuum. Arcs may be ignited and sustained over a wide range of chamber pressures.

Vacuum arc deposition technology employs a vacuum arc to generate vapour emission from the cathode with high energy atoms to be deposited on a substrate to form the coating.

Hard carbon films with diamond-like properties could constitute an interesting application of this technology. Such thin films have been deposited using ion beams [1-5] of carbon impinging on a substrate surface and resulting in carbon deposition.

A limiting factor in applying the vacuum arc deposition technique relates to the deposition of macro-particles. For many applications, however, the presence of any macro-particles is unacceptable. Much progress has been made, during recent years, in producing films that, while not completely free of particles, are a significant improvement on the films that were produced at earlier stages. Because the emission of micro-droplets (that become macro-particles in the deposited film) is of great significance in the deposition of thin films using VAD technique, it is the main aim for this study.

This study provides preliminary results on the generation mechanism of the particles found on the substrate under low pressure. Also some results on the size and population of these particles are obtained from this study in order to control the emission process of the particles. Scanning electron microscopy (SEM) and Auger electron spectroscopy (AES) are used to analyze the morphology and the structure of both particles and films. An image analyzer software is used to analyze the size and the number of the particles. The temperature effect of the cathode spot on the size and number of particles is studied in this work. The temperature values are calculated theoretically from a simplified model described in section 2-2-2.

CHAPTER - 1 -

1-1 : VACUUM ARC DEPOSITION

1-1-1 : WHAT IS VAD ?

Vacuum arc deposition (VAD) technique is an ion plating method that depends on the effect of high-energy ion bombardment to produce films that are both highly adherent and dense.

VAD technique is a physical vapour deposition (PVD) technique which employs a vacuum electric arc to generate vapour emission from the cathode. Ionized vapour of the cathode material is deposited onto the substrate, which is normally biased negatively with respect to the chamber and anode as shown in Figure (1-1). Arcing may be initiated by applying a high-voltage pulse to an electrode placed near the cathode (gas discharge ignition) and/or by mechanical ignition. The arc is diffused between electrodes and is sustained by the material originated from the cathode.

Evaporation occurs as a result of the presence of cathodic arc spots with very high current density (10^4-10^8 A/cm^2), small diameter (10^{-8}-10^{-4} m) and very short lifetime,typically 1 μs [6]. The high current density causes flash evaporation of the source material. The flux emitted from an arc source figure (1-2) consists almost entirely of ions and micro-droplets.

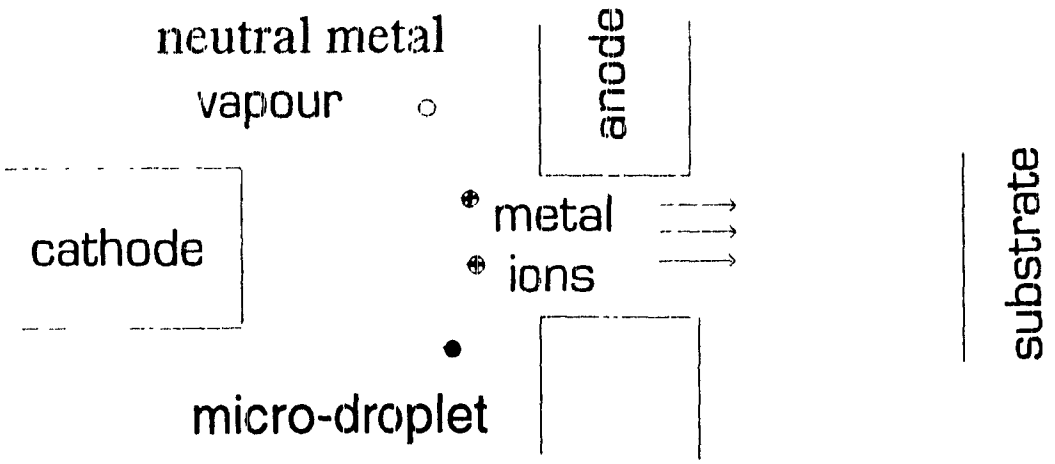

Figure (1-1): vacuum arc deposition system

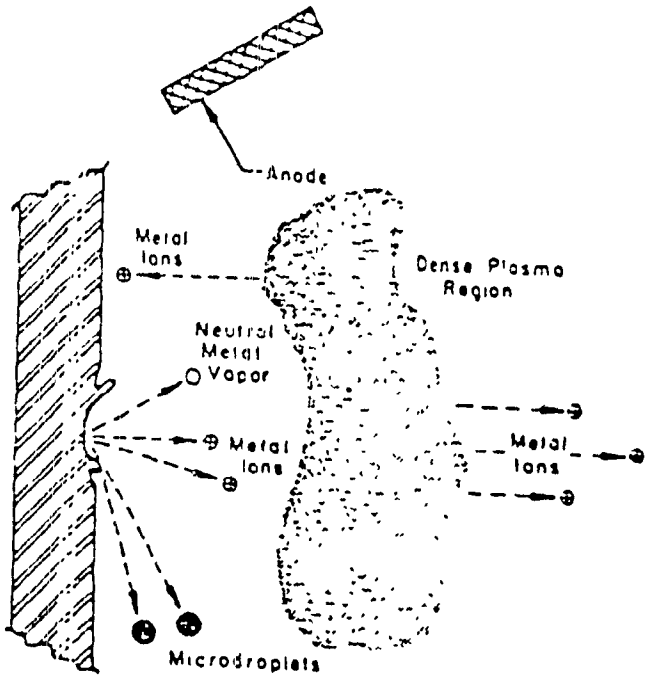

Figure (1-2) : Cathode spot region of a vacuum arc[7]

A major advantage of the VAD method is the high degree of ionization of the emitted material, it is widely acknowledged that neutral metal vapour constitutes only a small fraction (1-2%) of the mass transfer. The majority of the micro-droplets are emitted from the cathode at low angles (0°-30°) while the ions are emitted predominantly in a direction perpendicular to the plane of the cathode.

VAD was used in high vacuum where the ions directly bombard and penetrate the surface of the substrate. It is now used also for reactive deposition in which the ions produced by the cathode spots interact with the molecules of the background gas to form a compound coating on the substrate.

1-1-2: BASIC VAD SYSTEM

The basic VAD system is shown in figure (1-3). It consists of a vacuum chamber, cathode, anode, arc power supply, arc igniter, and a substrate which is usually negatively biased. A high-voltage pulse or mechanical trigger connected to the anode is used to ignite the arc. The arc is typically produced by applying an arc voltage of 15-50 V and an arc current of 30-400 A between the electrodes. The arc is sustained by the eroded cathode material.

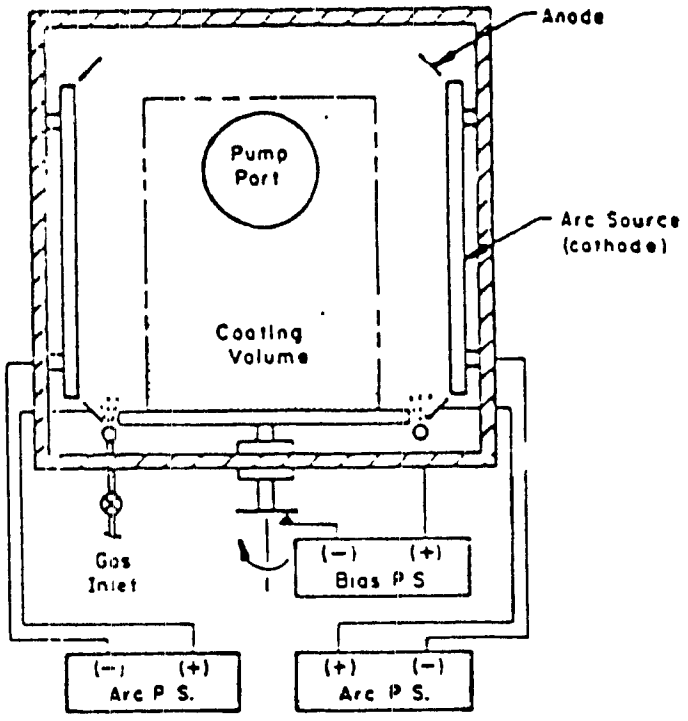

Figure (1-3) : A basic VAD coating system[7]

Different geometries are possible for this technique as shown in figure (1-4).

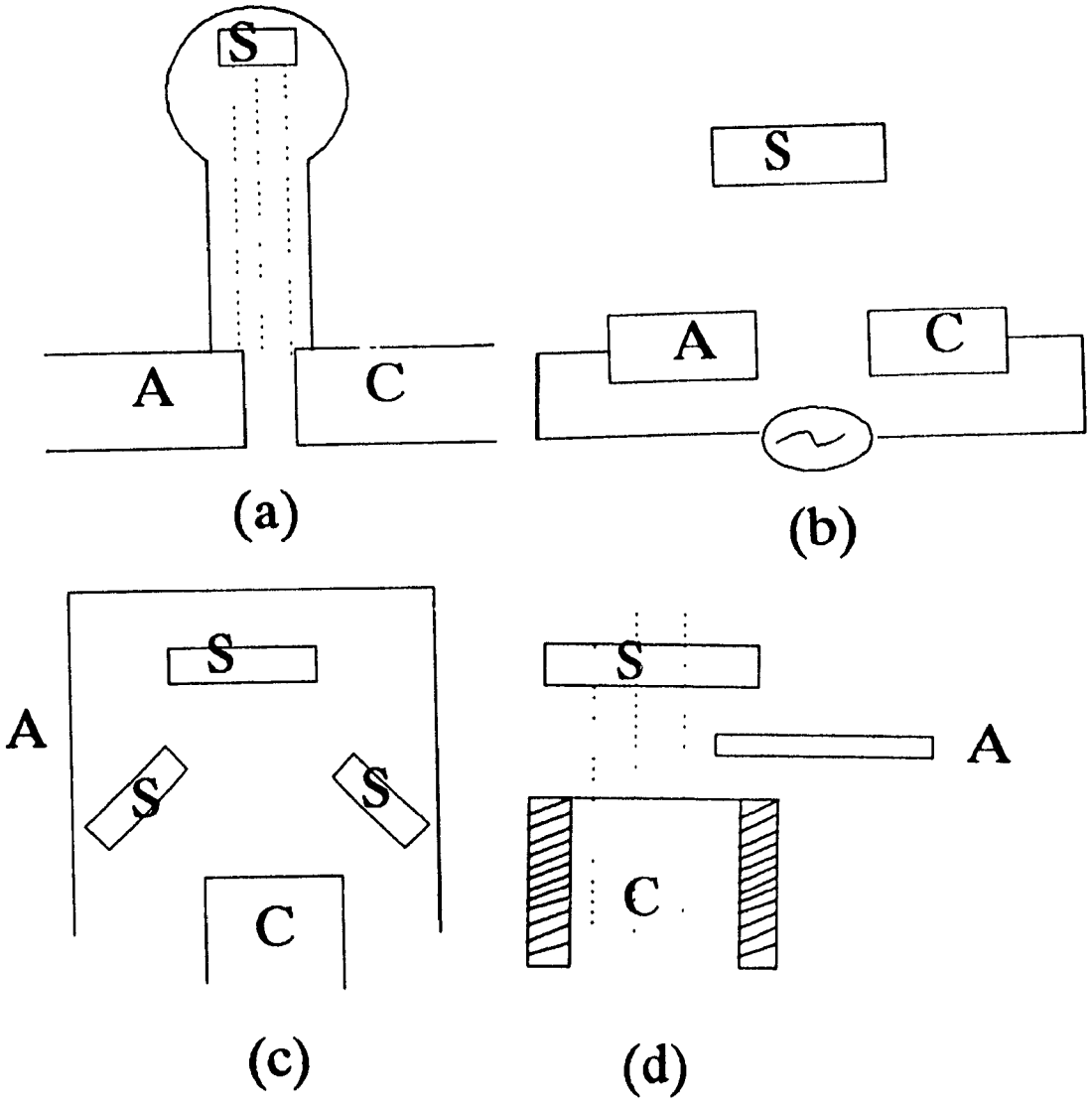

Figure (1-4) : Schematic representations of coating apparatuses with different geometries.
A=anode, C=cathode, S=substrate, the broken lines indicate the magnetic field, and the hatched areas are insulators[8].

1-1-3 : SOME CHARACTERISTICS FEATURES OF VAD [9]

VAD process uses the arc cathodic spot to generate the material plasma. Most of the vapour becomes ionized in the region of high power density adjacent to the cathode spot surface.

Flux intensities larger than many hundreds of the mA/cm^2 [10] can easily be attained in VAD while other ion beam deposition systems generate fluxes that are less than 10 mA/cm^2, however, Such high fluxes may be unfavourable in terms of coating quality. A compromise is thus needed for good film quality and high deposition rates.

Ion energy is a very important parameter for diamond-like films deposition in most techniques. Conventional thermal evaporation produces atoms with energies in the range 0.1 to 0.6 eV while sputtering produces atoms with energies in the range 4.0 to 10 eV. This level of deposition energy may still be too low for highly protective advance ceramic coatings.

Only 0.1% to 1.0% of the atoms are ionized in the basic ion plating processes. The majority of the depositing species in evaporative and sputter ion plating processes are neutral with low energy. This means a weak bonding deposition or a need of high substrate temperature.

In VAD techniques most of the material that is evaporated from the cathode surface is ionized (30%-100% depending on the cathode material) and associated with high kinetic energy in the 10-100 eV

range. This may result in deposits of high quality and high density.

VAD does not rely on substrate heating but instead relies on high energy ion bombardment to obtain high adhesion & density films.

VAD technique involves low costs compared to the sputtering system. This is due to the high efficiency of ionization and high energy of these ion. It is also due to the relative simplicity of VAD equipment compared to ion beam processes.

VAD can offer much higher deposition rate(μm/min) compared to sputtering (μm/hr). This is because of the large ion fluxes associated to the cathode spots emissions.

Good quality films can be deposited throughout a wide range of deposition parameters, the main one being pressure. Sputtering processes showed a difficult and very precise control of pressure was needed.

VAD can use any electrically conductive material as a cathode.

A depositing surface with no oxides, impurities, oil, grease, etc., is very important for good coatings. Cleaning inside the vacuum chamber prevents any re-contamination before deposition.

The most important problem for VAD is the deposition of micron-size particles on the films, that degrade film properties, such as density, hardness, chemical inertness, etc. Vacuum arc deposition is still a growing technology, to date however sputtering techniques are more widely used (essentially because of

the particle problems).

1-1-4 : VACUUM ARCS ON CARBON CATHODES

For the carbon cathode, with a residual pressure within the vacuum chamber below 10^{-6} torr, the following data are obtained from literature.

The current that can be carried by a single spot appears to be limited, and depends on the cathode material, for example, the maximum current per spot for carbon is 200 A. The number of spots is proportional to the arc current [11].

The cathode voltage drop across the space-charge region immediately adjacent to the spot has values in the range 10-30 V depending on the cathode material. For carbon, the cathode voltage drop is approximately equal to 16 V [11]. Figure (1-5a) shows the potential distribution [12] with the electrode surfaces at x=0 & x=d for a plasma positioned between two opposing electrodes at zero voltage. However when the electrode at d is made strongly positive, the electrons in the space charge region are drawn to the anode surface. Other electrons that arrive at d from the plasma body cannot accumulate because of the positive potential of the electrode surface, thus are continuously collected as a current. As a result the plasma potential rises to closely approach the potential of the anode, as indicated in figure (1-5b). The voltage distribution is independent on the distance between the cathode and the anode.

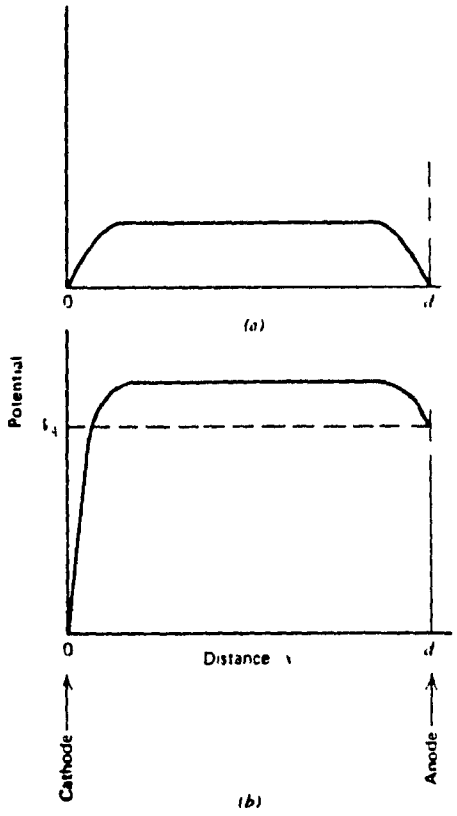

Figure (1-5) : The distribution of potential as a function of position between two conducting boundaries enclosing a plasma volume for a) two conducting boundaries at the same potential and b) two metal surfaces that differ in potential by V_a[12].

Figure (1-6) shows voltage-current characteristics of low current vacuum arcs using ten different cathode materials as measured by Davis and Miller [13]. The slope of the voltage current characteristics in vacuum is always positive with a very small value, typically for carbon dV/dI = 0.0094. This means it is possible to use multiple sources for deposition connected in parallel to generate multiple cathode spots.

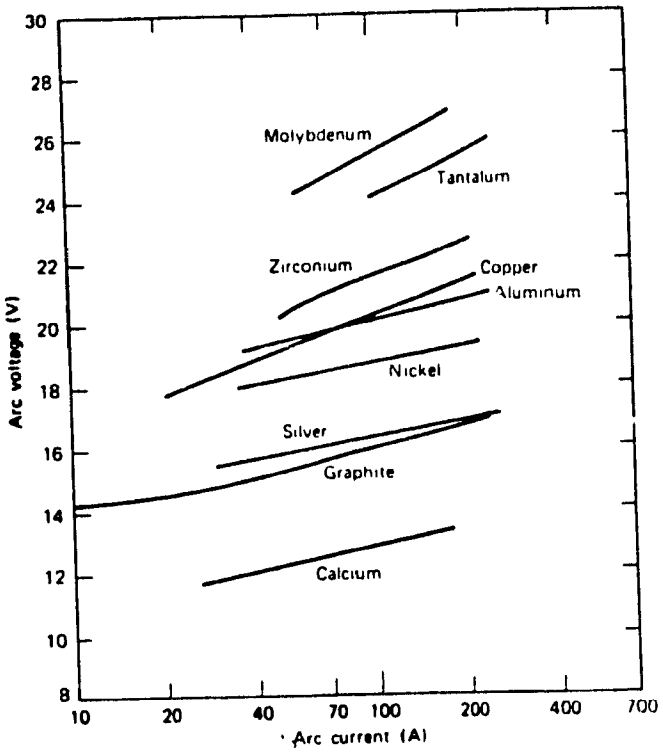

Figure (1-6) : DC-volt-ampere characteristics of vacuum arcs measured by Davis and Miller[13].

As already mentioned, a high degree of ionization is achieved by VAD technique. For carbon cathode, 70 % of the emitted vapour is ionized [6]. The ion charges are predominantly z=+1 (96%) and z=+2 (4%), as shown in Figure (1-7). This figure gives results for the most probable values of arc ion energy divided by ion charge (in units of electron charge) as a function of arc current for singly and doubly ionized cathode ions [13].

The erosion rate for carbon cathode measured by Kimblin is 1.7 x 10^{-5} gram/coulomb [6]. This value depends, however, on the cathode material and cathode surface structure. Graphite cathodes are porous materials and have high boiling point temperature. There exist a high probability that the arc will find a preferred location and simply remain there. The erosion rate will be higher than that for the non-porous and low boiling temperature cathodes. Because of the porosity, there may be a strong temperature gradient through the cathode material adjacent to the spot. This may cause thermal shock effects producing a mechanical removal of the material on a surface collecting these particles, this effect should produce particles of non-spherical shape and chunks.

The current density at each of the individual cathode spots lie in the range 10^{4}-10^{8} A/cm^{2} , with spot size in the range 10^{-8}-10^{-4} m, and lifetime of one microsecond [6].

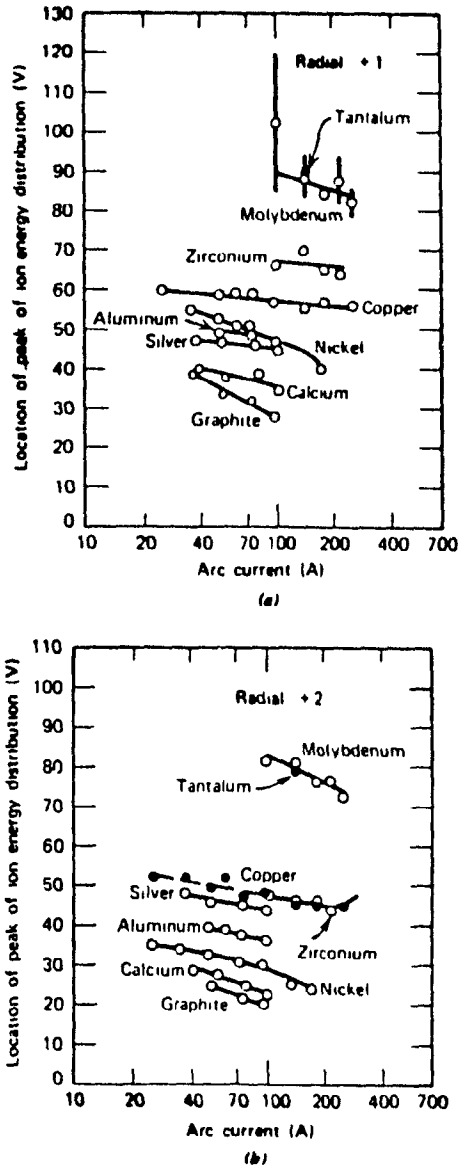

Figure (1-7) : Most probable energies of a) singly charged and b) doubly charged ions from vacuum arcs on several cathode materials[13].

1-2 : DROPLETS

1-2-1 : LITERATURE REVIEW ON DROPLETS

The literature tells us that the origin of the particles observed in vacuum arcs is the cathode, but no description is given of the micro-spheres observed from graphite cathode. Furthermore, the structure of these spheres has never been analyzed.

The results from M.Douyon de Azevedo[14] seem to indicate the spheres are made of multi-crystalline diamond. Private communications from different researchers speculated also that diamond crystals may also be found in the particles eroded from graphite cathodes. As in other vacuum arc systems, a probable origin of these micro-spheres could be the cathode spot region.

In this context, the following literature review on droplet emission from cathodes made of different materials can help to clarify the origin of the micro-spheres from a graphite cathode.

Utsumi[15] investigated the micro-droplet / macro-particle component of the emission from Au, Pd and Mg arcs. The velocity distribution of the micro-droplets was determined using a rotating vane velocity separator, and the size distribution was determined from direct measurement of deposited particles on glass slide substrate. Utsumi determined that for arc current in the range of 2-6 A, micro-droplets size ranged from a few hundred angstroms to several microns in diameter. It was noted that the ratio of volumes

carried by the particles and the vapour depended strongly on the cathode material. The percentage of the volume transported by micro-droplets for Mg, Pd and Au was found to be 80%, 50% and 10% respectively, that is, the percentage decreased with an increasing melting point temperature of the cathode material.

Tuma et al.[16] studied the spatial and size distribution of micro-droplets emitted from a copper cathode with an arc current of 80 A. Glass slides were used to intercept the emitted flux at low angles from the cathode and to determine the number and size of the macro-particles. Particles ranging in size from 1 μm to 10 μm in diameter were detected. The diameter of larger particles was difficult to measure because of the distortion that occurred on impact, smaller particles had solidified before impact.

The number and size of the micro-particles are dependent on the cathode material. Materials with higher melting points emit more ions and fewer micro-droplets. Once the cathode material is selected, the number and size of micro-droplets in the coatings are influenced by cathode to substrate geometry, arc current, magnetic field, gas species and pressure. Since micro-droplets are emitted at low angles relative to the cathode surface, the choice of coating system geometry will influence the concentration of micro-droplets on the substrate[7].

Daalder[17] observed the shape and density of the deposited particles from copper cathodes by the analysis with a scanning electron microscope (SEM). The particle number as a function of

particle size were counted from SEM photographs. The individual volume of the deposited particles was determined by a microscope (for surface examination) whose construction made it possible to measure dimensions both in the plane of and perpendicular to a target disc.

The angular mass distribution in particle form is peaked in the cathode plane (whereas the ion mass distribution is peaked perpendicular to the cathode plane)[18]. For increasing angles (positive and negative) this mass output rapidly diminishes. Large sized particles are dominantly represented in the mass flux having a small angle with the cathode plane, whereas for larger angles the smaller sized particles are representative. Figure (1-8) shows the angular distribution of particle mass flow from the cathode of a copper arc[18].

Aksenov et al.[19-20] used a method for eliminating macro-particles, they used a plasma optic system to deflect the path of the particles in the emission flux. The plasma optic comprised a curved metal tube having a longitudinal magnetic field of several hundred oersteds and a radial electric field of tens of volts. It was demonstrated, by studying the quality of the deposited films, that the ions could be successfully separated from the macro-particles and that particle-free coatings could be produced. Measurements of the radial ion current density profile at the exit of the plasma optic system indicated at a high degree of ions focusing along the axis of the system. Neutral atoms and micro-

droplets, their paths unaffected by the magnetic and electric fields, followed linear paths and were collected on the inner surface of the curved duct.

Yoshikatsu[21] used a technique to avoid the involvement of these particles, he applied a magnetic field on the top of the ion source to bend the flow of the ions, then the deflection ions were deposited on the substrate.

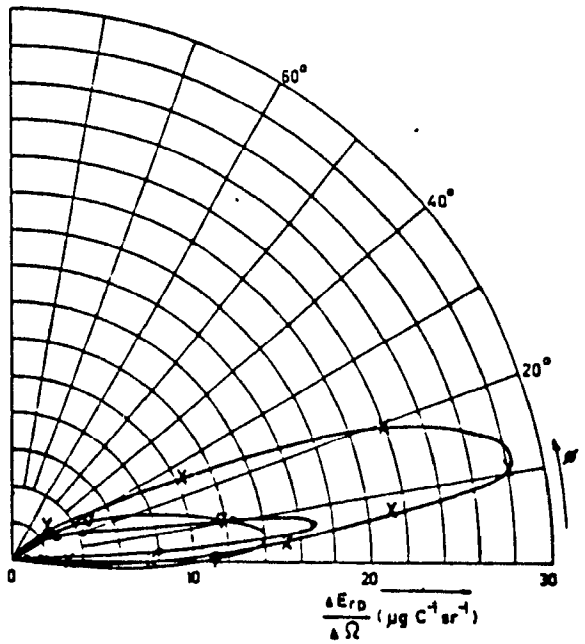

Figure (1-8) : Angular distribution of particle mass emission in a vacuum arc on a 25-mm diameter copper cathode. The angle is with respect to the cathode plane and taken from the cathode centre[17].

1-2-2 : PREVIOUS WORK ON VAD CARBON FILMS AT McGILL

Low pressure plasma is a noval area of study at McGill's Plasma Technology Research Centre. A master's student, Mario Douyon de Azevedo, has previously worked in the field of deposition using vacuum arc deposition (VAD). The project, supervised by Professor Jean-Luc Meunier, dealt with the study of angular distribution and ionic flux intensity measurements when depositing carbon by VAD technique.

M.Douyon de Azevedo studied the intensity of the ion flux with distance to cathode and background gas pressure, these two parameters playing a major role on the film quality by modifying the flux intensity and energy. Gas pressure influences not only the cathodic ion flux properties, but it can also affect the erosion rate of the cathode[22].

In vacuum the ionic flux decreases with distance as the solid angle covered by the probe. Increasing the hydrogen pressure decreases the ionic flux collected at a given position.

Some important observations of preliminary deposition conducted by M.Douyon de Azevedo and J.-L.Meunier are shown in figures (1-9 to 1-11).

Figure (1-9a) shows the micro-spheres that appear on the film under the following deposition parameters : $P=10^{-2}$ Pa, T_s= 470 C and V_{bias}= -300 V where P is the background hydrogen pressure, T_s is the substrate temperature and V_{bias} is the applied potential to the

substrate. Also large plates with uniform appearance were formed. These plates show cracking along preferential directions and the incorporation of micro-spheres. The cracking and the poor adhesion of the film is essentially due to a film thickness that is too large (several microns) to sustain the strong internal stresses. Figure (1-9b) shows a close-up of Figure 1-9a with the structure of spheres imbedded in the deposit. These spheres do not appear on films with the same arcing conditions but varying deposition parameters.

Figure (1-9): a) SEM recording of a deposit made on tungsten in vacuum($P=10^{-2}$ Pa) with T_s=470 C & Vs=-300 V.

b) Close-Up of (a) showing the structure of spheres imbedded in deposit[14].

Figure (1-10) shows an AES spectrum of a deposit made on Tungsten in vacuum ($P=10^{-2}$ Pa), T_s= 470 C & V_s=-900 V. Typical AES spectra of diamond, graphite and amorphous carbon films are shown for comparison. The typical structure of diamond can be seen. This result and the structure observed in Figure (1-9b) leads one to believe that these micro-spheres are of similar nature as the diamond balls produced in low density deposition experiments using a high carbon/hydrogen atomic ratio[23].

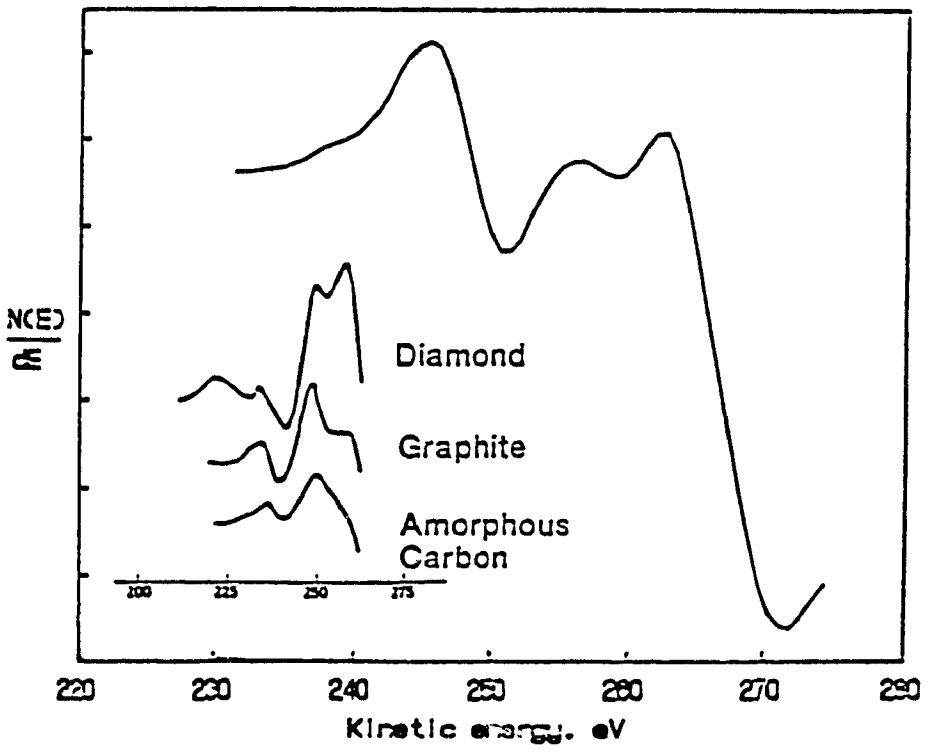

Figure (1-10) : AES spectrum of a deposit made on Tungsten in vacuum($P=10^{-2}$ Pa) with T_s=470 C and V_s=-900 V[14].

The typical and most convincing signature stating the presence of diamond is given by a Raman peak located at 1332 cm^{-1}. Raman is not a sensitive test to detect diamond in the presence of other types of carbon[24]. Figure (1-11) is a Raman spectrum of a deposit made on Nickel in vacuum $P=10^{-2}$ Pa with T_s= 470 C & V_s= 0 V. This Figure shows a small peak at 1332 cm^{-1} superposed over a broad background covering a wide range of intermolecular distances up to the strong graphite peak at 1584 cm^{-1}. Considering that the Raman scattering cross-section on diamond crystals is much smaller than the one for graphite, we may conclude this Figure shows the presence of micro-crystals with diamond structure imbedded in a matrix composed of amorphous carbon with graphitic domains.

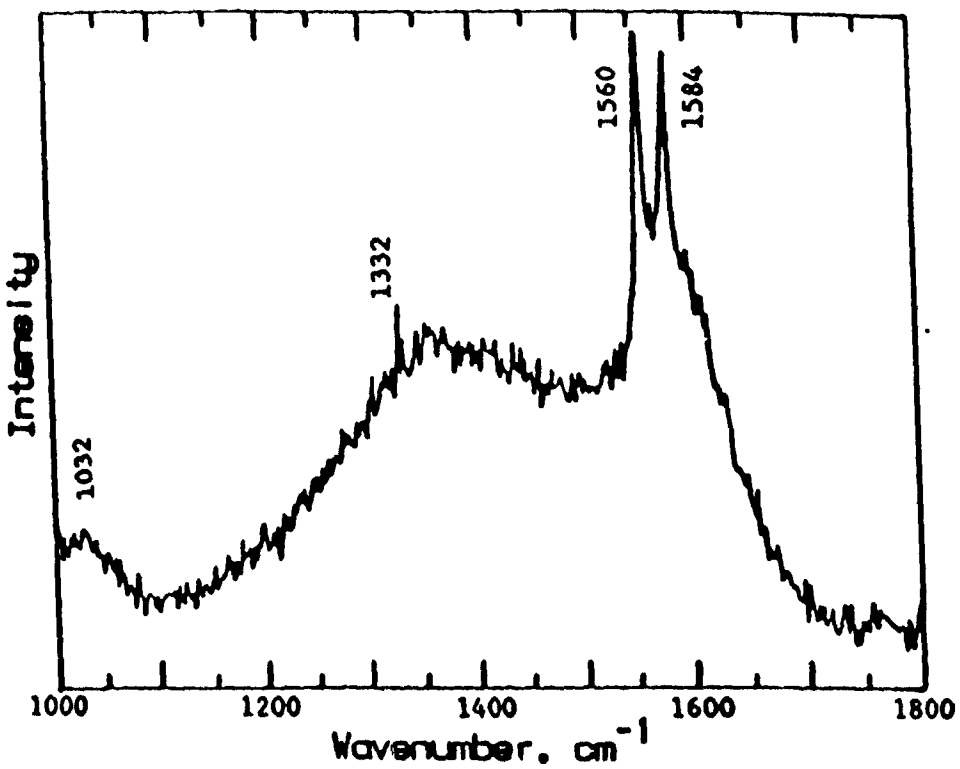

Figure (1-11) : Raman spectrum of a deposit made on Nickel in vacuum($P=10^{-2}$ Pa) with T_s=470 C & Vs=0 V[14].

The above results indicated that a large variety of films structures can be obtained by changing deposition parameters. Most importantly, these results stressed the importance of the droplets problem in VAD diamond-like film deposition. The diamond signature has also been identified, although at this point we do not know if this diamond structure was associated to the particles or the film itself. Raman spectroscopy alone cannot lead to a good enough spatial resolution to answer this question. The literature tells us that the origin of the particles observed in vacuum arcs is the cathode[18], but no description is given of the micro-spheres observed from graphite cathode. furthermore, the structure of these spheres was never analyzed. The results from M.Douyon de Azevedo seem to indicate the spheres are made of multi-crystalline diamond. As in other vacuum arc systems, a probable origin of these micro-spheres could be the cathode spot origin. At this point however, we must not discard the possibility of the diamond growth from the carbon ion bombardment at the substrate level. The resemblance of these micro-spheres with the thermal plasmas and CVD growth of diamond structures having a "cauliflower" appearance at high C/H ratio, and the fact that no micro-spheres were observed under different deposition conditions (different bias voltage and substrate temperature) could support this second hypothesis[10]. Decreasing the C/H ratio improves the quality of the deposit with the sharp diamond line in the spectrum. When this ratio was decreased to its optimum value, the 1332 cm^{-1} fine band became the

only observable carbon band[24].

1-3 : CARBON

1-3-1 : DIAMOND AND DIAMOND-LIKE CARBON

The objective of the vacuum arc deposition technique using a graphite cathode is to produce hard carbon films having diamond-like characteristics. The following gives a short review of what is meant by diamond-like carbon.

Coatings which have high degree of SP^3 bonding generally have properties, especially hardness, close to those of single-crystal diamond and are often referred to as diamond-like carbon. Recently, large grain size diamond crystals and continuous diamond coatings have been prepared by plasma chemical vapour deposition methods.

The widespread realization of diamond coatings by vapour phase synthesis has occurred in the U.S.A and Europe only over the last 15 years. However it is now becoming clear that such an achievement is over a decade old in the Soviet Union and half a decade old in Japan. In addition, during this period, considerable effort has been placed upon another type of material commonly called Diamond-like carbon (DLC). The common denominator in stabilizing SP^3 carbon atoms in DLC has been ion bombardment of the growing film. These latter materials represent a broad range in structure (primarily amorphous with variable ratio of SP^2 to SP^3 bonding) and composition (variable hydrogen concentration).

The term diamond-like carbon was coined by Aisenberg and Chabot in 1971 [25], it covers a wide range of materials including both amorphous and micro-crystalline atomic structures and coatings anywhere from 0 to more than 30 % H. Unfortunately, there has been essentially no distinction made among these materials using structural and compositional criteria.

It is interesting to note that natural diamond may also contain considerable amounts of impurities of "dopants", e.g., nitrogen, hydrogen or boron. As the crystallite size falls below 0.2 micrometer the definitive characterization becomes more difficult and the distinction between diamond and diamond-like carbon coatings is tenuous. When increasing the total energy delivered to the growing surface, the film character shifts from polymer-like, soft deposits to DLC films, at very high energies graphitization is observed. This means that only a certain range of energies give rise to the DLC structure, characterized by a high ratio of the SP^3/SP^2 hybridizations present in the micro-structure and containing substantial concentration of hydrogen.

The properly adjusted energy flux during film growth gives rise to properties such as high density, hardness, chemical inertness and low coefficient of friction. Typical ranges of values and parameters are summarized in Table(1-1).

*TABLE (1-1) : BASIC CHARACTERISTICS OF a-C:H FILMS [26]**

Structure	*Multiphase system :* *amorphous diamond-like (SP^3)* *amorphous graphitic (SP^2)* *amorphous polymeric (SP^1)* *compared to : Diamond : Crystalline*
Hydrogen concentration	*20 - 50 %* *compared to : Diamond : < 0.1 %*
Density	*1.5 - 2.0 g/cm³ (high conc. of H)* *2.0 - 3.4 g/cm³ (lower conc. of H)* *compared to :* *Glassy carbon : 1.5 - 1.55 g/cm³* *Graphite : 2.3 g/cm³* *Diamond : 3.5 g/cm³*
Electrical properties	*Conductivity : 10^{-10} - 10^{0} (Ω cm)$^{-1}$* *compared to : Graphite : 10^{2} (Ω cm)$^{-1}$* *Diamond : 10^{-18} (Ω cm)$^{-1}$*
Microhardness	*10 - 50 GPa* *compared to : Graphite : 24 GPa* *Diamond : 70 GPa*

* *a-C:H : Hydrogenated amorphous carbon (diamond-like)*

1-3-2 : APPLICATIONS OF DIAMOND-LIKE FILMS

On account of their unique characteristics, a-C:H films have been proposed for a number of applications, examples of which are listed in table (1-2) :

TABLE (1-2) : SUMMARY OF PROPOSED APPLICATIONS [26]

a-C:H films :
- corrosion and abrasion resistant coatings.
- anti-reflection coatings for IR optics (i.e., for Ge at 10.6 μm) and solar cells.
- tribological applications, protection against severe environments (sand, salt water).
- dry lubricants.
- hermetic barrier coatings on optical fibers and on suboptical memory discs to give longer life times.
- laser writing (change in conductivity upon irradiation from 10^{-6} to 10^{+1} Ωcm).
- biocompatible material for protection, and for promoting cell growth.

1-4 : OBJECTIVES

The first objective of the present study is to obtain an evidence on the origin of the spheres that appear on the substrate surface during the vacuum arc deposition processes using a graphite cathode. The structure of these particles are analyzed using a diagnostic technique with high enough spatial resolution, the Auger electron spectroscopy (AES).

The second objective is to establish if the droplet emission mechanism can be correlated to thermal effect in the cathode spot. For this, we control the cathode surface temperature using the arc current intensity and arcing time. Droplet emission under different thermal load to the cathode are measured.

CHAPTER - 2-

-1 : EXPERIMENTAL SET-UP

CO_2-TEA LASER

A pulse arc system was used to control precisely the arc time. The temperature of the cathode surface can be controlled by controlling the arc current intensity and arcing time. This control may help us to establish if the droplet emission mechanism can be correlated to the thermal effect in the cathode spot.

In the present work, a high voltage CO_2-TEA laser pulse (mixture of 80% He, 10% N_2, and 10% CO_2) was used to ignite the arc. Such a laser provides the high precision needed in time compared to a mechanical device, and does not produce the strong electrical noise of high voltage triggering systems. It produces an infrared radiation at 10.6 μm with high power of approximately 1 MW and a short duration time of 200 ns. As shown in figure(2-1a), the laser beam was send to a Germanium (Ge) mirror, which reflected the beam to Zinc Selenium (ZnSe) lens with a 25 cm focus distance. The beam entered the vacuum chamber through a salt window permitting the infrared radiation to pass. It was focused on the tip of the cathode where the arc burns.

ELECTRICAL CIRCUIT

The electrical circuit system shown in figure (2-1a), is used in this work. The electric arc current is generated by the discharge of a capacitor bank (C1=38 mF), charged using the power supply PS1 (6448B DC Power Supply, Hewlett-Packard, 0-600 V, 0-1.5 A). The current then passes through the first thyristor (T1), which is responsible for the initial trigger time of arc t_i, then to the anode and cathode circuit. The duration of the arc current can be adjusted from 10 μs to 10 ms by using the second thyristor (T2) which switches off the capacitor bank by the use of an electronic "crow bar circuit" using capacitor (C2) charged using power supply PS2 (same model as PS1 but with reverse polarity). Therefore, thyristor T2 triggering signal is responsible for the shut off time t_f of the arc current. The duration of the arc pulse was monitored using an oscilloscope.

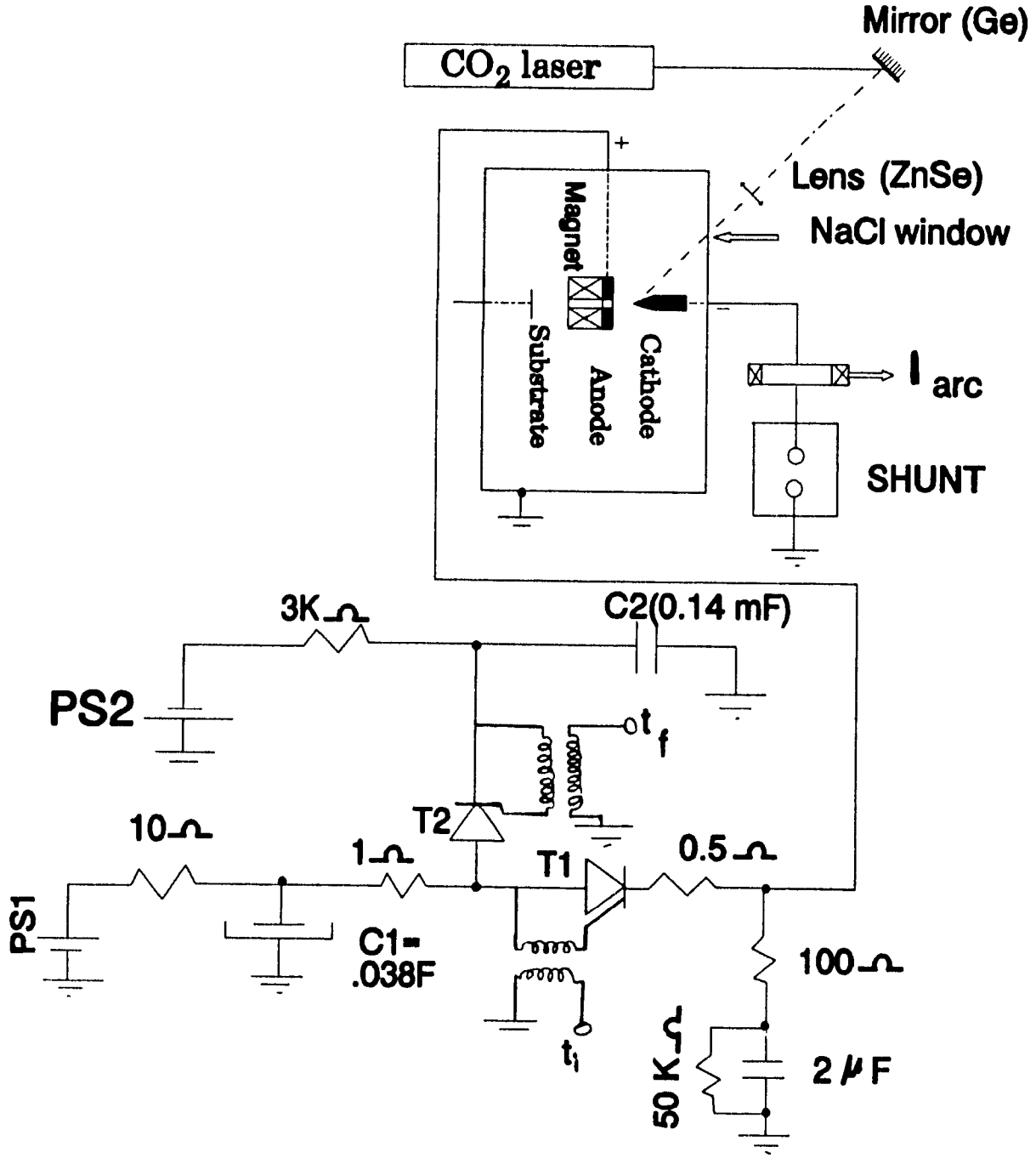

Figure(2-1a): Geometry and electrical circuit

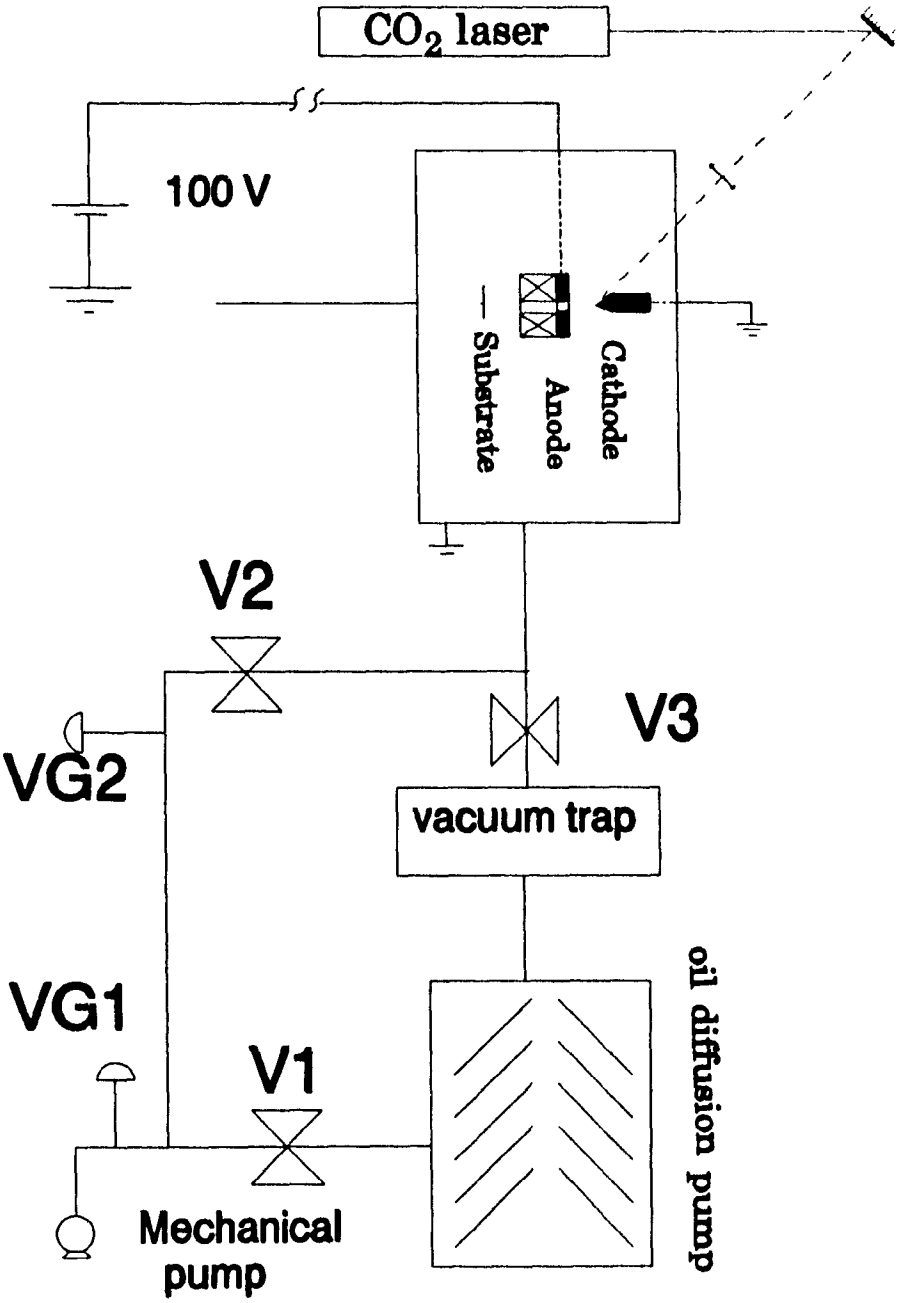

Figure (2-1b) : Vacuum Chamber and Pumping Arrangement

CURRENT MEASUREMENT

*The arc current was measured using a Pearson pulse current transformer No. 411 (0.1 V/A) connected to an oscilloscope type 549 Tektronix. This was useful for short arc duration times, but not useful for long arc duration times. The pulse current transformer saturates at Q = I*t = 0.19 C. This implies the current transformer does not give any signal once the 0.19 C limit is exceeded and hence we were not able to monitor the long duration times. For this reason, we were forced to use a shunt to monitor the arc current for long arc times. The shunt is in series with the circuit and shows some inductance. This produces a lot of electrical noise at the high dI/dt occurring at the on and off triggering times of the arc. The shunt, however, works very well in the constant arc current period with low dI/dt as shown in figure (2-2). For these reasons, both the Pearson pulse current transformer and the shunt are used to measure the arc current.*

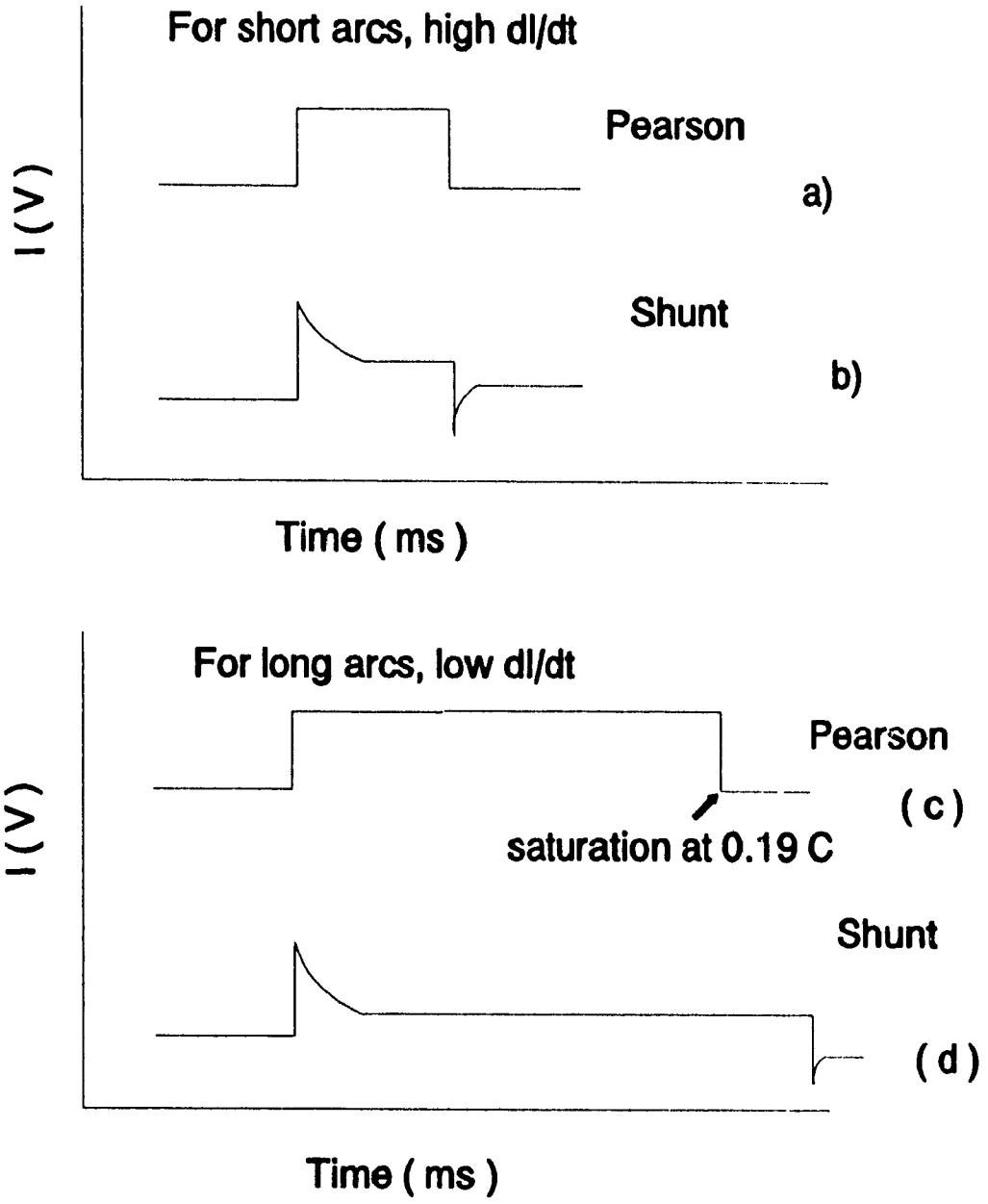

Figure (2-2): Representation of an oscilloscope signals

for a) Pearson current transformer for an arc with Q≤ 0.19 C.
b) Shunt for an arc with Q≤ 0.19 C.
c)Pearson current transformer for Q > 0.19 C.
d) Shunt for Q > 0.19 C.

ELECTRODES

One can see in Figure (2-3) the electrodes arrangement used in this experiment. The cathode (on the right in Figure 2-3) is a small graphite rod 12.7 mm in diameter and 25.4 mm in length, tapered by arc erosion with time. The graphite cathode according to manufacturer's specifications had an impurity content of 10 ppm. The anode is a graphite circular disc of 50.8 mm in diameter. It has a hole in the centre of 12.7 mm in diameter through which the emitted vapour from the tip of the cathode can pass to be deposited on the substrate. The thickness of the anode is 9.5 mm. The distance between the cathode and the anode is 5.0 mm, and both were connected to copper rods serving as vacuum feed through and electrical supply connectors.

Small magnets are attached to the back of the anode in order to increase the amount of the deposition on the substrate. For each diagnostic technique, a certain amount of deposition should be on the substrate. These magnets forced the ions to travel along the magnetic lines toward the substrate.

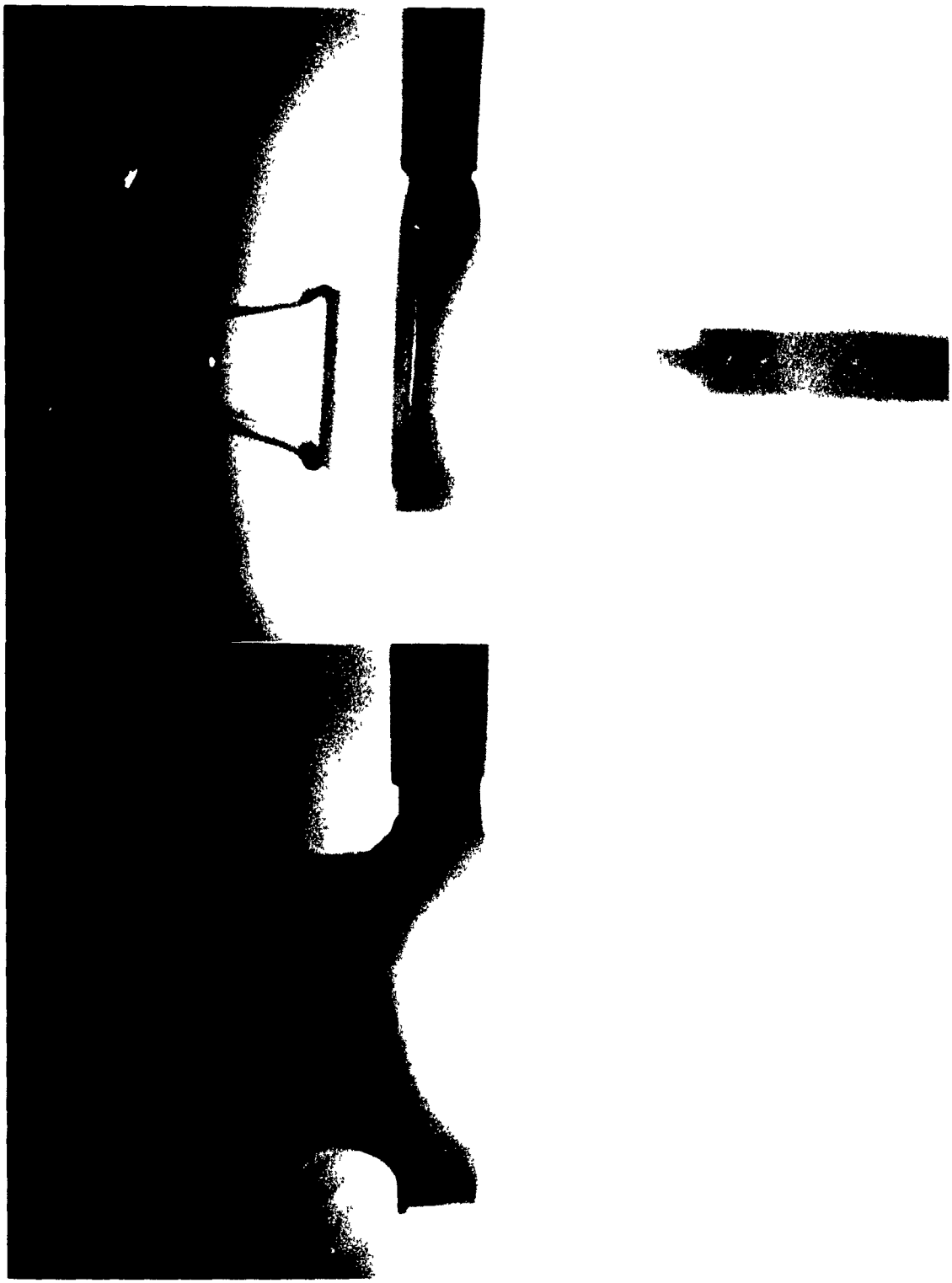

Figure (2-3) : Graphite cathode and graphite anode

SUBSTRATE

Three kinds of substrates are used in this work.

a) Microscopic Glass Slides of 1x25x25 mm.

This was the first choice because of the cheap price. The problem for using this substrate is that the glass accumulates charges inside the SEM during analysis of the deposits. This means, each sample should be coated before using SEM.

b) Aluminum Specimen Mount with a 12.7 mm diameter flat surface and a 3.2 mm back pin.

This was the second choice. The problem with this substrate was the bad finishing surfaces which made it difficult to recognize the deposited particles clearly.

c) Silicon Wafers of 12.7 mm diameter and 21 Mills thickness.

This substrate was the final choice. Both sides were polished which means good surface finishing for analysis. They were semiconductor, meaning no charge accumulated on the substrate and no need for coating for SEM analysis.

PUMPING SYSTEM

The vacuum pressure inside the chamber is produced by using a mechanical and an oil diffusion pumps as shown in Figure (2-1b).The pressure was measured by using a) PIR 1A PIRANI UNIT which can measure pressures from 10^{-1} torr to 10^{-3} torr and b) GIC-300 Ionization Gage which can measure pressures from 10^{-3} torr to 10^{-8} torr. The pressure was constant during this work and equal to 10^{-4} torr. This is well below the onset of pressure effects affecting the erosion rate of the cathode[27].

2-2 : EXPERIMENTAL PROCEDURE :

2-2-1 : DEPOSITION EXPERIMENT :

The first step in the experimental procedure was the preparation of the sample. In general, in all deposition processes the initial preparation of the substrate is very important because the cleaning of the substrate plays a critical role in the quality of adhesion between the substrate and the coating.

In this investigation, however, cleaning the substrate surface was not so important because we were not interested in the deposited layer itself or in the adhesion quality.

The second step was producing the desired vacuum pressure of 10^{-4} torr inside the chamber by using the diffusion oil pump.

The third step was producing the arc between the cathode and the anode in order to vaporize the cathode material and deposit the vapour on the substrate. During the deposition process the pressure was constant, and the intensity of the arc current could be adjusted between 44 A to 110 A by changing the voltage on the capacitor bank shown in Figure 2-1a. The arc time was changed from 2.5 ms to 14 ms and controlled by using the second thyristor in the electric circuit and monitored by using a shunt and an oscilloscope.

The distance between cathode and substrate could be adjusted between 7.5 cm and 45 cm.

2-2-2 : TEMPERATURE DISTRIBUTION

One objective of this study is to correlate the number of emitted particles with the surface temperature of the cathode. Surface temperature, however, is a very difficult parameter to estimate, even more to measure. The cathode for, example, will have extremely different surface temperatures at the cathode spots of the burning arc compared to the unaffected area away from these spots. These randomly moving spots of typically 10^{-8}- 10^{-4} m in diameter, of lifetimes in the micro-second range and showing very strong plasma radiation prohibit any classical measurement method.

We may however obtain information on the evolution of the particle emission with temperature through a control of this surface temperature by varying the arc duration. The pulsed system with very short and controllable arc durations showing square current pulse shapes was chosen for this reason. What is needed in this study is essentially the relative evolution of surface temperature for different arcing current I and arc time t.

In order to study the effect of the cathode spot temperature on the micro-particles, a simple heat transfer model is suggested. It is first assumed that the cathode spot affected zone has a cylindrical shape with diameter d and length L (Figure 2-4a). The diameter of the cathode spot is assumed equal to a certain value in the range of the spot size, for example ($5x10^{-4}$ m) [6]. We assumed also that all the electrical power is used to heat this cylindrical

volume only. For vacuum arcs on graphite electrodes the maximum current per spot reaches a value of 200 A before any spot splitting occurs[11]. This value is always smaller than the current used in this study, we can thus suppose only one cathode spot is burning at a given time during the experiment. For our calculations, we will suppose this spot always burns at the same location throughout the total arcing time. This should lead to strongly overestimating the temperature. However, the typical lifetime of a spot is relatively constant and always smaller than our arc duration time, and the short values of arcing times used do not permit movement of the spot over a wide area. Hence this assumption should not have a strong effect on the relative value of temperature for two arcing conditions. We will also neglect the effect of phase transformations of the carbon at the surface.

Radiation from the surface of the cathode spot seems to be a strong heat loss mechanism because of the high temperatures reached in this zone. One must consider, however, that the cathode spot does not face a vacuum ambient, but on the contrary, a dense, optically thick and highly radiating cathodic plasma. We will suppose this high density plasma layer above the cathode spot to act as a blackbody at the same temperature as the surface, hence eliminating radiation losses of the surface.

All these assumptions greatly simplify the problem, the temperature can now be evaluated by using the simple heat transfer equation

$$q = m\ Cp\ DT \qquad \text{..... (2-1)}$$

where $q = IxVxt$ .....(2-2)

I : is the arc current, A

V : is the arc voltage, V

m : is the heated mass, Kg

Cp : is the specific heat of the cathode(graphite), KJ/Kg.K

DT : is the temperature change from 293 K to T

t : is the arc duration time for a square pulse shape, s

The mass m is equal to the density of the cathode multiplied by the volume of the heated material (spot volume= $\pi d^2 L/4$).

The length L is determined by using the simple heat conduction equation

$$q = k\ A\ dT/dL \qquad \text{..... (2-3)}$$

where k is thermal conductivity coefficient of the graphite which is function of temperature. After integration of equation (2-3), we notice that the temperature decreases gradually with increasing length until $L = 5x10^{-3}$ m. This length is assumed to be constant for any T_s for simplicity. After this length the temperature can be considered constant (Figure 2-4b).

Using equation (2-1) and the above values for d & L, the temperature T_s of the cathode spot as a function of the arc current and duration time is shown in figure (2-5).

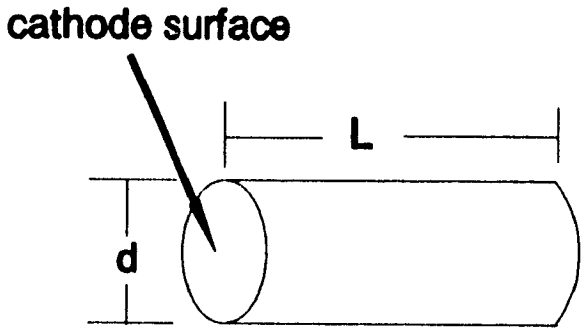

Figure (2-4a): Schematic for heated volume on the cathode surface

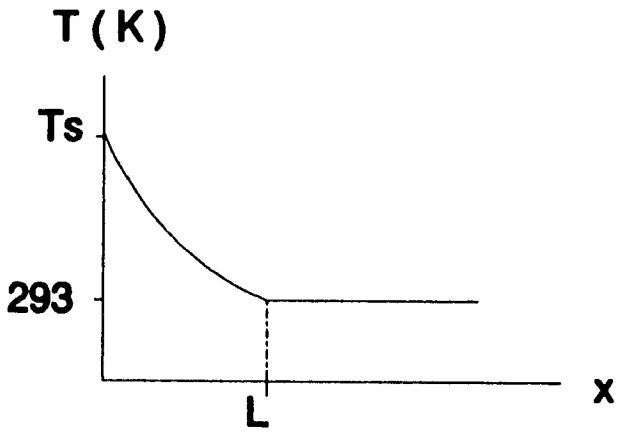

Figure (2-4b): Effect of conductivity througth the cathode

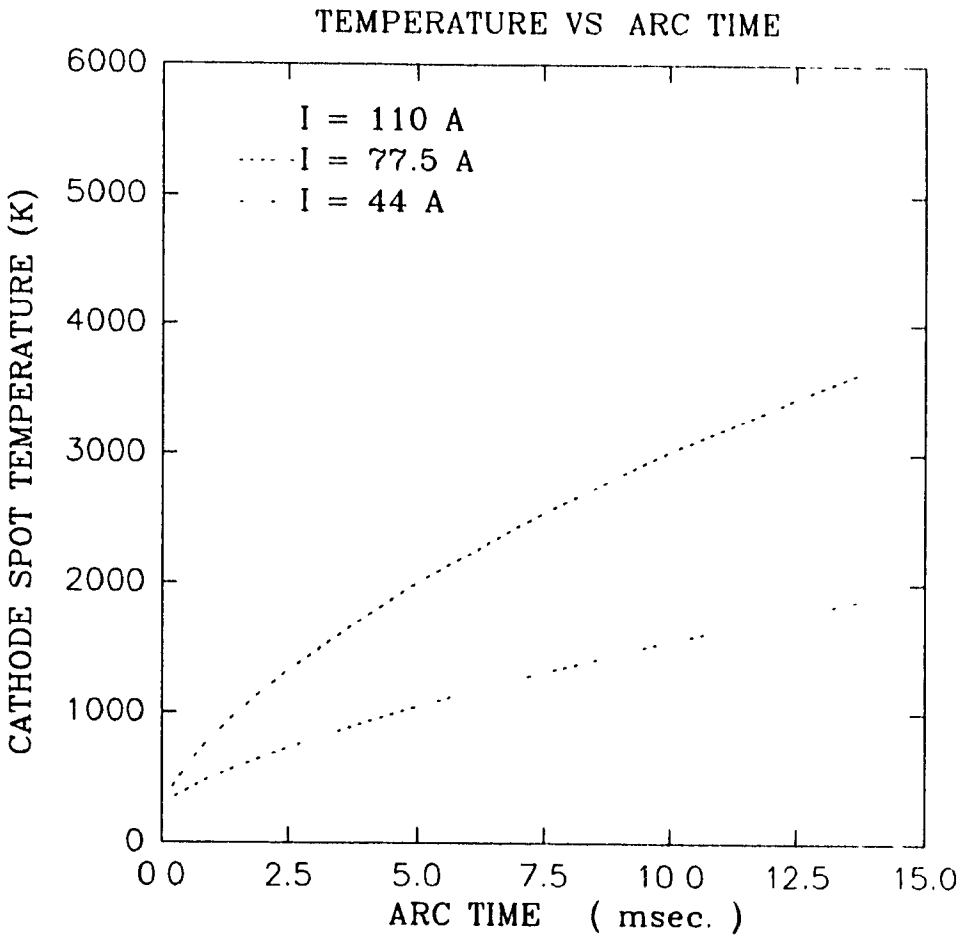

Figure (2-5) : Cathode spot temperature T_s as a function of arc time for I=110 A, 77.5 A, & 44 A, calculated from eqn.2-1.

2-2-3 : COOLING TEMPERATURE CURVE

The period between each arc ignition must be long enough to allow the cathode spot to cool to room temperature, otherwise, the cathode spot temperature will increase gradually after each ignition. To avoid this problem, a simple model is used to evaluate the cooling time of the spot after arc extinction. In order to be on the safe side, only the conduction heat transfer mode is again considered. This leads to overestimating the required time.

The temperature distribution in a body with unsteady state conduction is given by Fourier's general law of heat conduction :

$$\frac{dT}{dt} = \frac{k}{\rho C_p}\left[\frac{d^2T}{dx^2} + \frac{d^2T}{dy^2} + \frac{d^2T}{dz^2}\right] \qquad 2\text{-}4$$

where : T : Temperature at any point given by x,y,z.

t : cooling time.

k : Coefficient of thermal conductivity.

Cp : Specific heat of unit mass.

ρ : Mass per unit volume.

α : Thermal diffusivity (= $k/\rho Cp$)

Assume that at t=0, the temperature distribution is uniform at room temperature T_0 = 293 K, for all x (before arc ignition). If the temperature of the cathode surface is suddenly altered to T_s (just after arc ignition), then (after the arc extinction) the rate of the heat flow q/A past any plan aa (due to cooling effect) may

be assumed to depend upon the change in surface temperature T_s-T_o, the distance x from the surface to the plan, the time t during which the temperature change has existed due to the cooling effect, the thermal diffusivity α, and the coefficient of thermal conductivity k.

By applying the π theorem for dimensionless analysis (see for example ref.28) to these variables it is seen that

$$\pi=\phi[(\frac{q}{A})^a(T_s-T_o)^b x^c \alpha^d t^e k^f]$$

After equating the exponents to zero yield the equations:

$$\pi_1=q\frac{\sqrt{\alpha t}}{A(T_s-T_o)k}$$

$$\pi_2=\frac{x^2}{\alpha t}$$

$$\phi=\phi(\pi_1,\pi_2)=0$$

$$T_s=T_o+[\frac{q\sqrt{\alpha t}}{Ak}\frac{1}{f_2(\frac{x^2}{\alpha t})}] \qquad 2\text{-}5$$

where, q/A is the rate of heat flow past any plane aa after t second. Values of the dimensionless function $f_2=(x^2/\alpha t)$ must be obtained experimentally or by some other type of analysis. In this case the values are given graphically in the curve of figure (2-7) [28], and can be obtained from the solution of Fourier's equation.

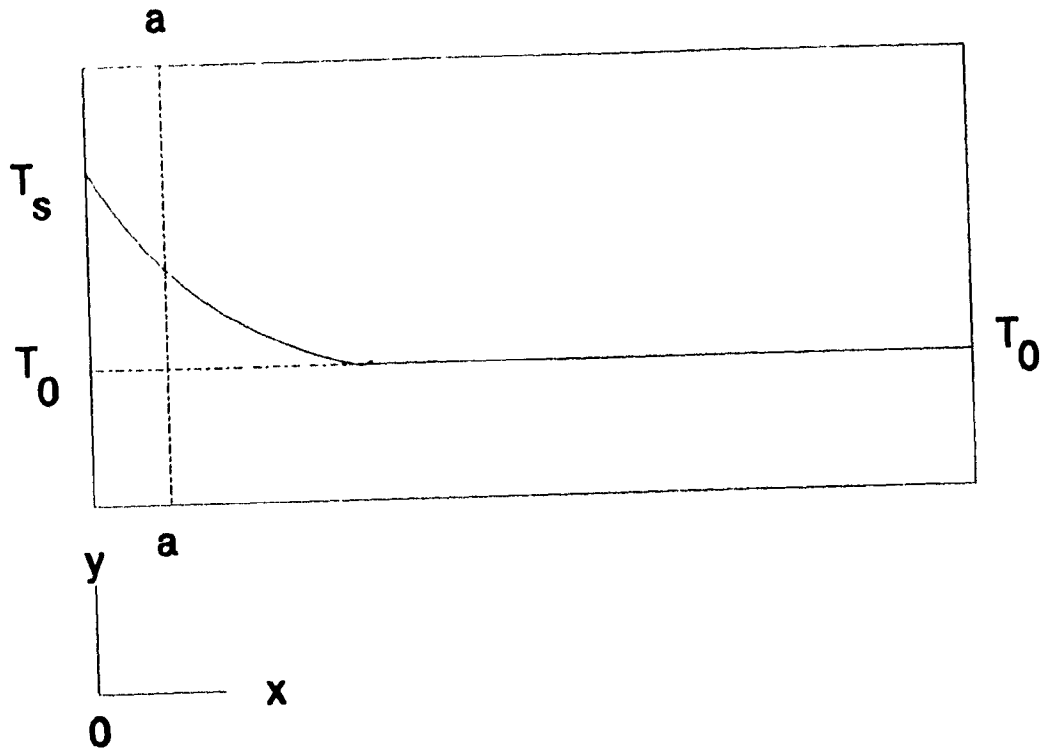

Figure(2-6) : Schematic distribution of the temperature through the cathode.

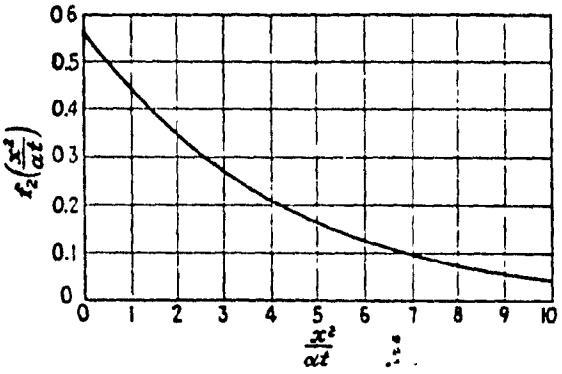

Figure (2-7) : Values of function f_2 used with equation 2-5 [28].

From the solution of equation (2-5), twenty seconds was good enough to cool the spot from T_s to 293 K, as shown in Figures 2-8, 2-9 and 2-10. If the radiation heat transfer is considered, these cooling times are expected to be much smaller than 20 second.

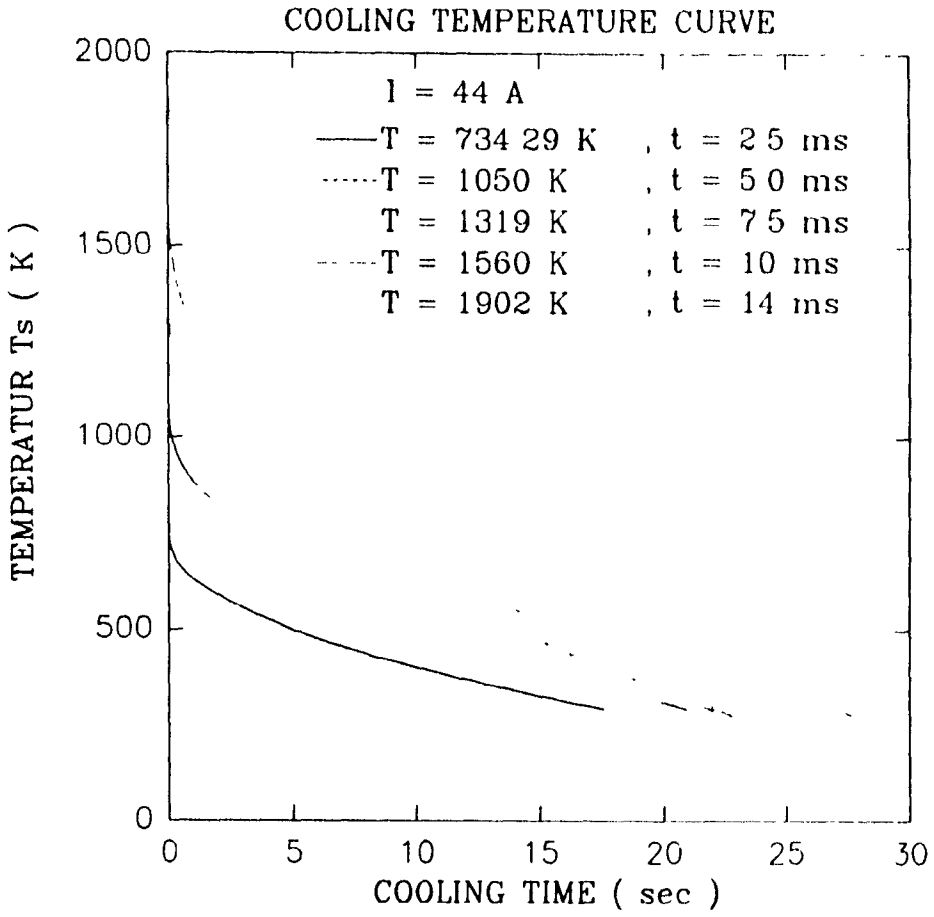

Figure (2-8) : Temperature of cathode spot surface as a function of the time for I=44 A, at x=0.

T = cathode spot temperature

t = arc duration time

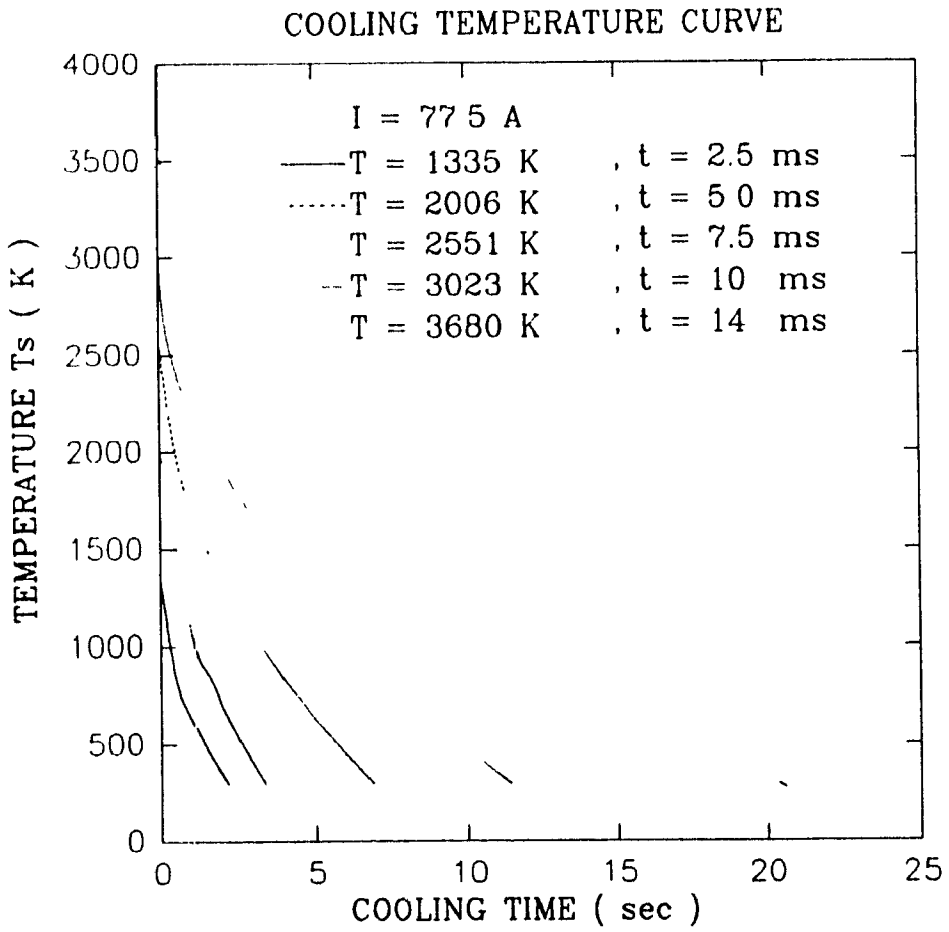

Figure (2-9) : Temperature of cathode spot surface as a function of time for I=77.5 A, at x=0.

T = cathode spot temperature

t = arc duration time

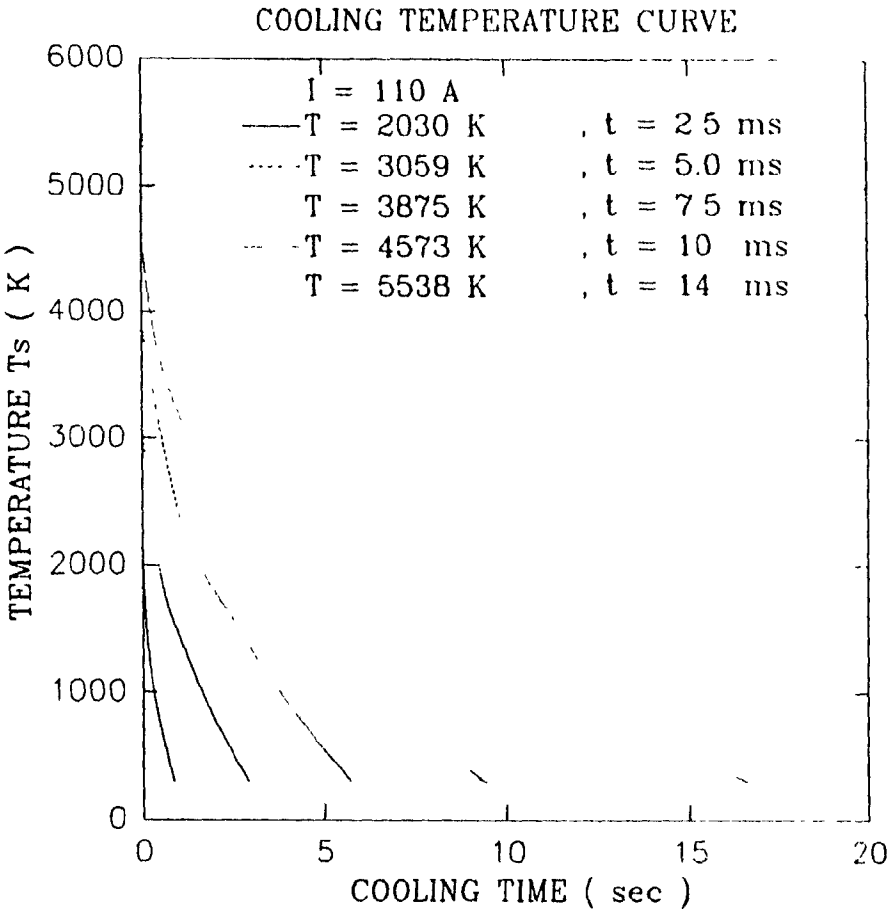

Figure (2-10) : Temperature of cathode spot surface as a function of time for I=110 A, at x=0.

T = cathode spot temperature,

t = arc duration time.

2-2-4 : PARTICLE DIAGNOSTICS:

The size and concentration of particles are measured by using an Image Analyzer Software connected to the Scanning Electron Microscopy. The typical sequence of operations that an image processor might go through are as follows:

To get an image from a sample into the memory of the computer, an image acquisition hardware is attached to a scanning electron microscope (SEM), the image is digitized into a black and white image. The shades of black and white, called grey-levels, represent intensity information. Image acquisition alone is not really image processing, but if we average several frames together, image enhancement is being done. Averaging of successive frames of data enhances an image by decreasing the relative intensity of noise. Once an image has been acquired, the intensity levels stored for each of the pixels (single dots in the image) can be modified to improve the visual effect. In a washed-out picture, the information may still be there but the difference is too subtle to be perceived. Exaggeration of these differences can result in a vast improvement in picture quality. This technique is known as contrast stretching. Another means of image enhancement is called filtering. In filtering, each pixel is replaced with a weighted average of its neighbours. Depending on the weighted average used, a filter can be applied to reduce high frequency noise, eliminate erratic points (both called smoothing), or accentuate edges (called sharpening).

Once a quality picture is obtained, the picture is stored. This stored image is however in a form which makes it difficult for the computer to distinguish an object from background. The term segmentation refers to the conversion of an image from grey level to binary. In a binary image, pixels corresponding to features of interest are either on or off. Segmentation requires a value judgement as to whether a pixel is part of the object or not. It should be apparent that errors may be made in the creation of a binary image. It may be necessary to join lines, fill holes, and disconnect separated objects. Binary filters or manual editing can accomplish this clean up. A binary image contains a compact description of what is object and what is background. Using the binary image, the computer can generate a variety of sizing parameters including areas, lengths, and widths, etc.

For each sample, five different areas of 1681 μm^2 each were analyzed. The number of the particles in each sample was evaluated by analyzing five different locations on each substrate, then taking the average of the number of particles from the five locations. The locations were four at the corners and one at the centre. The substrates for all measurements are located in the direction perpendicular to the cathode surface, on the main axis of the discharge. The range of the particle size that we used for counting was between 0.1 μm and 10 μm.

CHAPTER - 3 -

3-1 : EXPERIMENTAL RESULTS :

The following table shows all the operating conditions for all samples, where :

Q(C): is the number of charges passing through the cathode[Coulomb]

I(A): is the arc current [Ampere]

t(ms): is the arc duration time [milliseconds]

D(cm): is the distance between cathode and substrate [cm]

N(arc): is the number of arc ignitions

The pressure inside the vacuum chamber was constant $P=10^{-4}$ torr.

Table (3-1) : OPERATING CONDITIONS

SAMPLE	Q(C)	I(A)	t(ms)	D(cm)	N(arc)
1	30.8	110	14	7.5	20
2	61.6	110	14	7.5	40
3	92.4	110	14	7.5	60
4	123.2	110	14	7.5	80
5	154	110	14	7.5	100
6	30.8	110	14	13	20
7	61.6	110	14	13	40
8	92.4	110	14	13	60
9	123.2	110	14	13	80
10	154	110	14	13	100

continue

SAMPLE	Q(C)	I(A)	t(ms)	D(cm)	N(arc)
11	30.8	44	14	13	50
12	61.6	44	14	13	100
13	92.4	44	14	13	150
14	123.2	44	14	13	200
15	154	44	14	13	250
16	30.8	44	14	7.5	50
17	61.6	44	14	7.5	100
18	92.4	44	14	7.5	150
19	123.2	44	14	7.5	200
20	154	44	14	7.5	250
21	50	110	2.5	7.5	182
22	50	110	5.0	7.5	91
23	50	110	7.5	7.5	61
24	50	110	10	7.5	46
25	50	77.5	2.5	7.5	258
26	50	77.5	5.0	7.5	129
27	50	77.5	7.5	7.5	86
28	50	77.5	10	7.5	65
29	50	44	2.5	7.5	454
30	50	44	5.0	7.5	152
31	50	44	7.5	7.5	114
32	10	44	0.5	7.5	454
33	100	110	14	45	65

3-1-1 : NUMBER AND SIZE OF PARTICLES

The size and population of the particles in the carbon film are dependent on several factors. Some of these factors are studied in this work.

ARC CURRENT LEVEL :

To evaluate the effect of the arc current on the size and number of particles, the arc current is changed while the number of coulombs (IxtxN), the distance between cathode and substrate , and the arc duration time were constant. The number of coulombs, i.e., the total charge passing through the cathode per deposition experiments is used here as a parameter because in the literature the total erosion rate is usually expressed in grams per coulombs. For the low arc current values used here, it means the eroded mass is constant at a given charge to the cathode.

As the arc current delivered to the cathode is increased, as shown in figures (3-1) & (3-2), the number of particles at constant number of coulombs and constant distance between cathode and substrate is increased. In this case, keeping the total number of coulombs constant implies different number of arc pulses have been used for different currents.The same area of substrate for particle count was used for all conditions in Figures (3-1) and (3-2).

The arc spot has a very small size (10^{-8} - 10^{-4} m) and very high

current density (10^6 - 10^{12} A/m^2). This high local current density rapidly heats a small volume of the cathode surface (cathode spot), explosive evaporation occurs, and the cathode spot simultaneously migrates to another location to repeat the process[29]. As a result, the population of the emitted particles increases as the current level increases.

As mentioned already the erosion is directly proportional to the total charge passing through the cathode. Another important experimental result obtained by Kimblin[30] is the constancy of the ratio of the ion flux emitted by the cathode to the total current. A contradiction seems to exit between the results of Figure 3-1 and 3-2 and the two assertions above. Increasing the arc current at constant total charge should increase the ionic vapour emitted by the cathode while keeping the erosion rate constant. This should normally induce a decrease of the number of particles emitted. Our results do not agree with such a prediction and follow more a generation mechanism based on thermal effects.

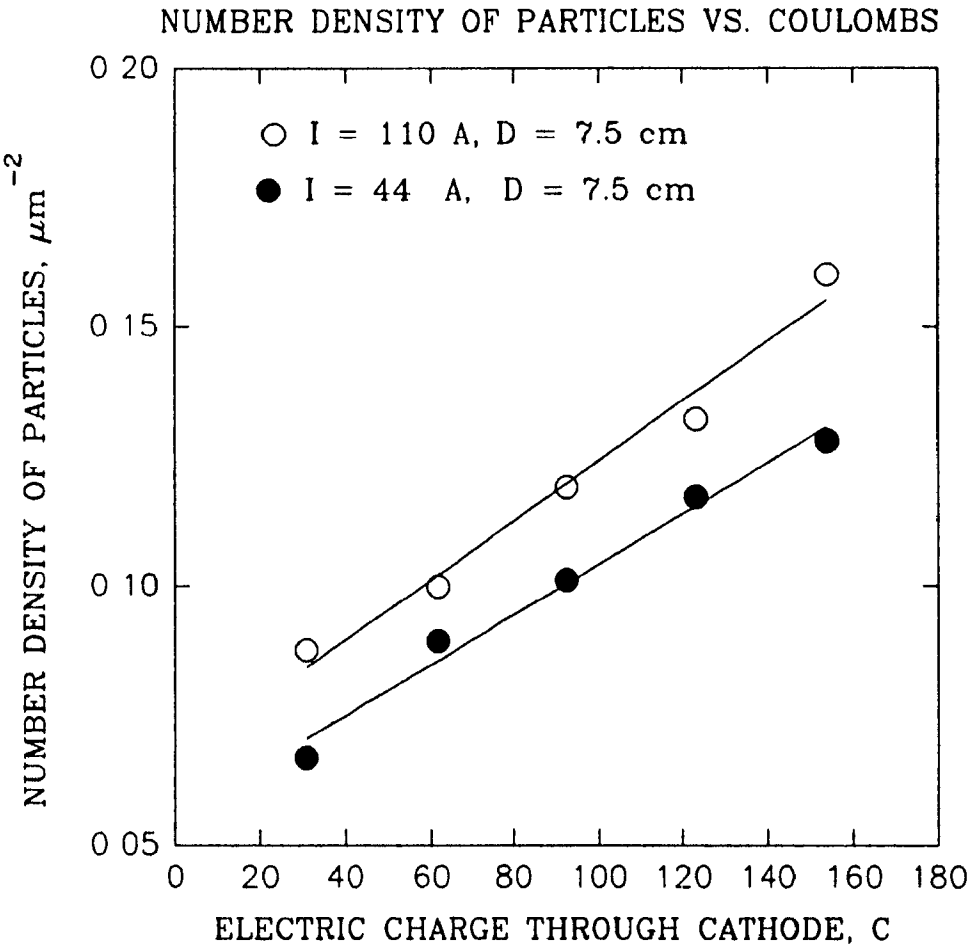

FIGURE (3-1) : Number density of particles as a function of electric charge through cathode for I=44 A and 110 A, D= 7.5 cm, t=14 ms.

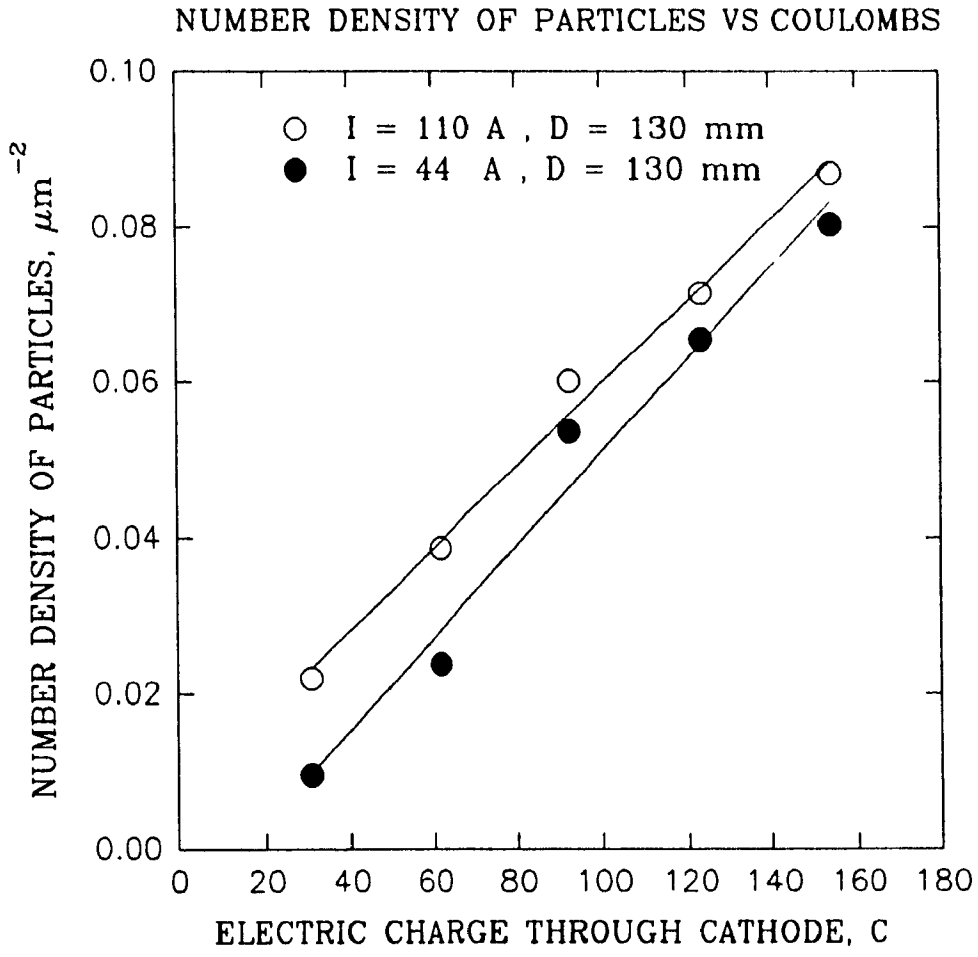

Figure (3-2) : Number density of particles as a function of electric charge through cathode for I=44 A and 110 A, D=13 cm, t= 14 ms.

DISTANCE BETWEEN THE CATHODE AND THE SUBSTRATE

To evaluate the effect of the distance between cathode and substrate, the distance was varied between 7.5 cm and 45 cm at constant number of coulombs and constant arc current.

Figures (3-3) & (3-4) respectively, show that the number of particles over a given substrate area decreases with increased distance between the cathode and the substrate. From these experimental observations we can note the following: by comparing the number of particles per μm^2 at 110 A, 100 C, and 14 ms but different distances between the cathode and the substrate, we found that $1.189*10^{-3}$ particles/μm^2 was found on the substrate that was at 45 cm from the cathode, $6.543*10^{-2}$ particles/μm^2 on the substrate that was at 13 cm from the cathode, and $1.249*10^{-1}$ particles/μm^2 at 7.5 cm. These values correspond to $1.189*10^5$ particles/cm^2, $6.54*10^6$ particles/cm^2 and $1.250*10^7$ particles/cm^2, respectively.

This decrease in the number of particles with distance between the cathode and the substrate should in fact correspond to the decrease of the solid angle of the substrate as viewed by the cathode (i.e., surface area of substrate divided by the square of the distance between substrate and cathode). Figure (3-5) is another plot of the data in figures (3-3) & (3-4) with vertical axis as number density of particles per unit solid angle. This figure shows that the particle density per solid angle remain approximately the same at different distances between cathode and

substrate. The error on the particles counting was approximately 5% according to the standard deviation of the averaging technique. However, the location of the cathode spot on the electrode may not necessarily be on a surface area that is perpendicular to the discharge axis. This would lead to different emission angles inducing large errors in the particle count. The curves of figure 3-5 for a given current value are thus considered within the same error margin. This means that, the particles travel along straight-lines.

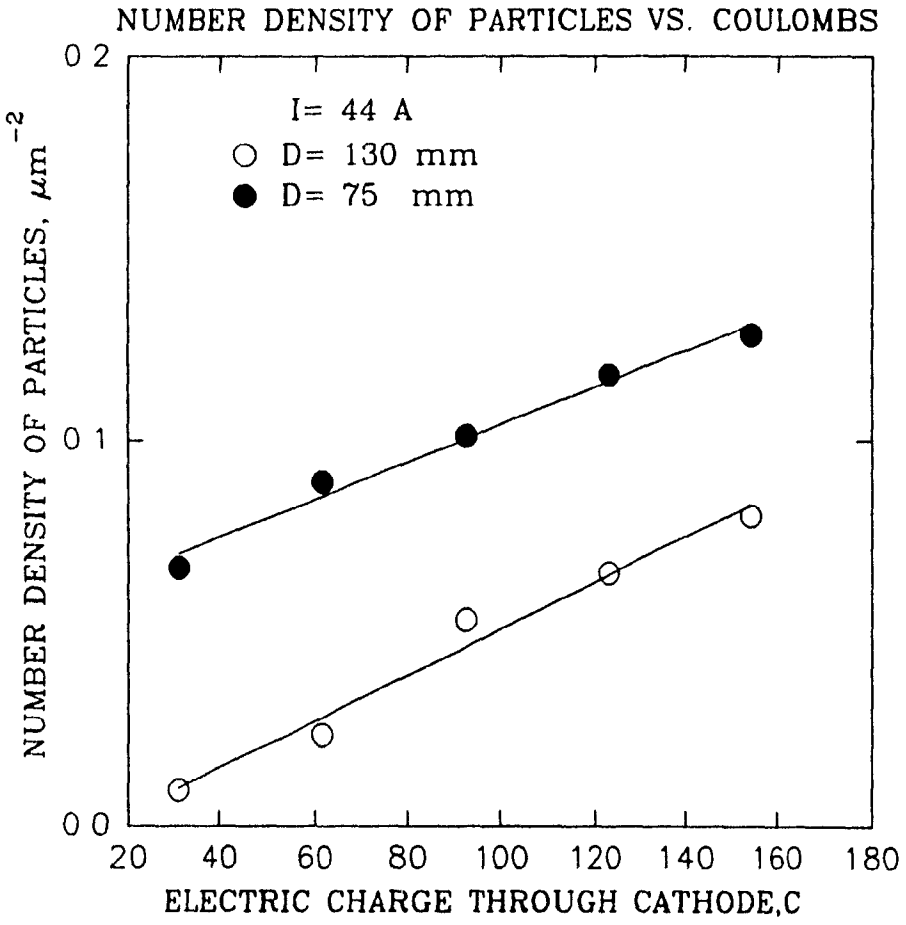

Figure (3-3) : Number density of particles as a function of electric charge through cathode for two distances between cathode and substrate, for I=44 A and t= 14 ms.

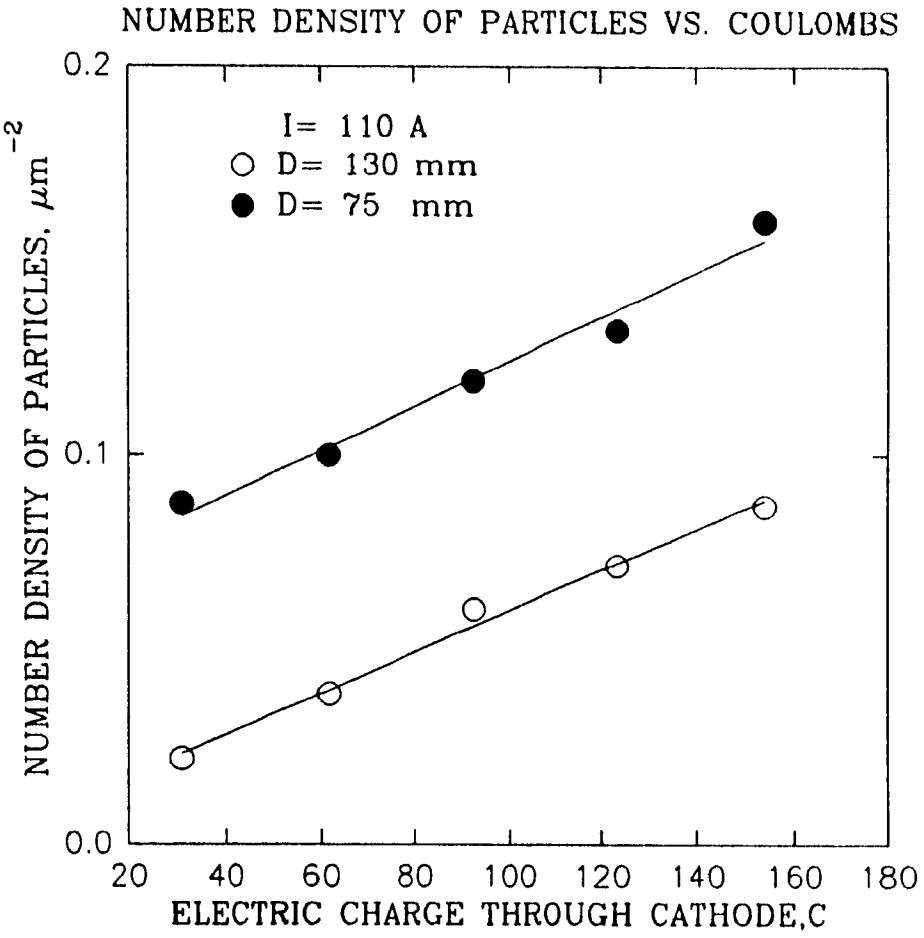

Figure (3-4) : Number density of particles as a function of electric charge through cathode for two distances between cathode and substrate, for I= 110 A and t= 14 ms.

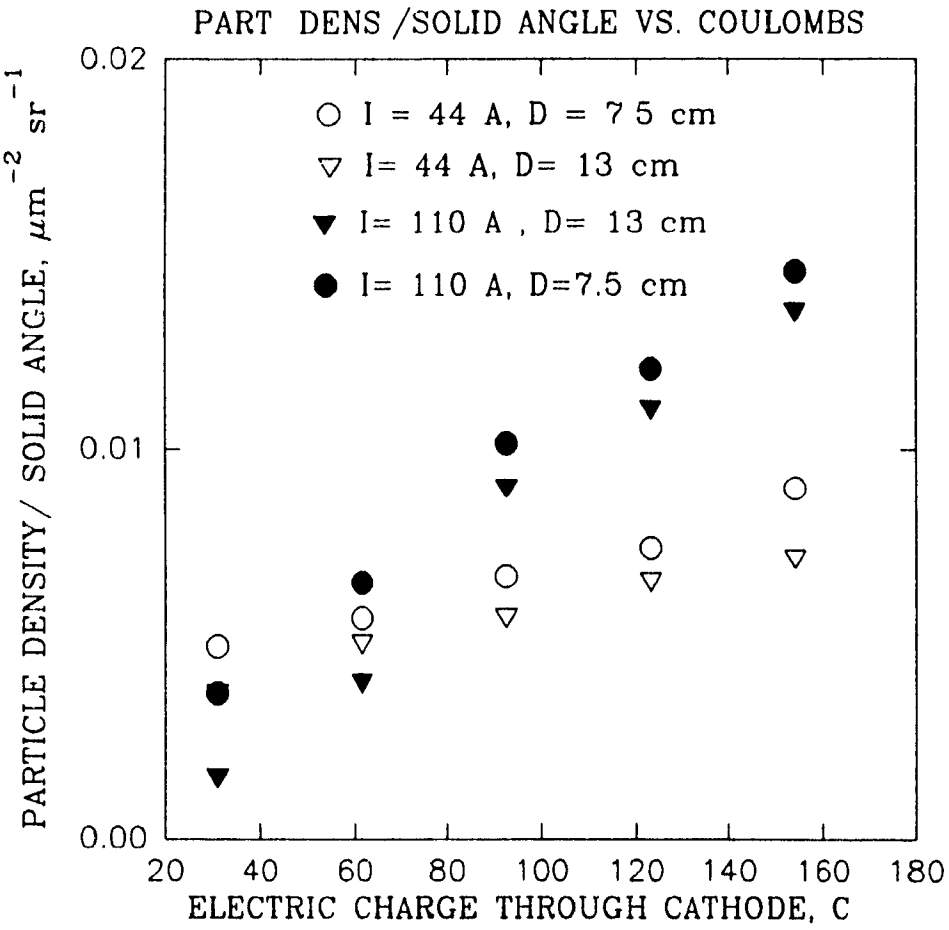

Figure (3-5) : Data of Figure (3-3) and (3-4) normalized to the solid angle of the substrate as viewed by the cathode.

ARC TIME

The arc duration time was controlled using the " crow bar circuit" shown in figure (2-1a), which allow us to control the arc time from 10 μs to 10 ms. To evaluate the effect of the arc time on the population of the particles, the arc time is changed while the arc current, distance between cathode and substrate and the number of coulombs were kept constant. In this case, the constant number of coulombs was attained by increasing the total number of pulses while maintaining a constant current.

A decrease in the arc duration time at a constant arc current should decrease the mean residence time of the cathode spot at any point and hence decrease the heat load to the cathode. The volume of the material that is melted and explosively emitted from the cathode spot should hence decrease with a decrease of the arc duration time. An increase in the population of the droplets emitted from the crater and deposited on the substrate as arc time increases is shown in figure (3-6). The range of the arc time shown in figure (3-6) is quite narrow (i.e., from 2.5 ms to 14 ms).
It would be interesting to evaluate the shape of this curve in the range from 0 to 2.5 ms, i.e., to see its evolution towards the very small arcing times. The reason of not carrying any experiment with these small arc times is the long time needed for each experiment. For example, if one wants to carry experiment at I=100 A, Q= 100 C and t= 0.1 ms, then the number of arc ignitions will be

10^4 arcs(N=Q/Ixt). As mentioned in section (2-2-3), the time period between each arc is 20 seconds. This means $2x10^5$ s or 55.55 hours are needed to carry one run leading to only one data point. A fully automated system would then be needed.

Nevertheless, the arc time range studied shows clearly relatively linear increases in the number of particles with arc time for constant total charge passing through the cathode. This result supports a particle emission mechanism induced by thermal effects. The next section will show a correlation of particle count with calculated values of the cathode spot temperature.

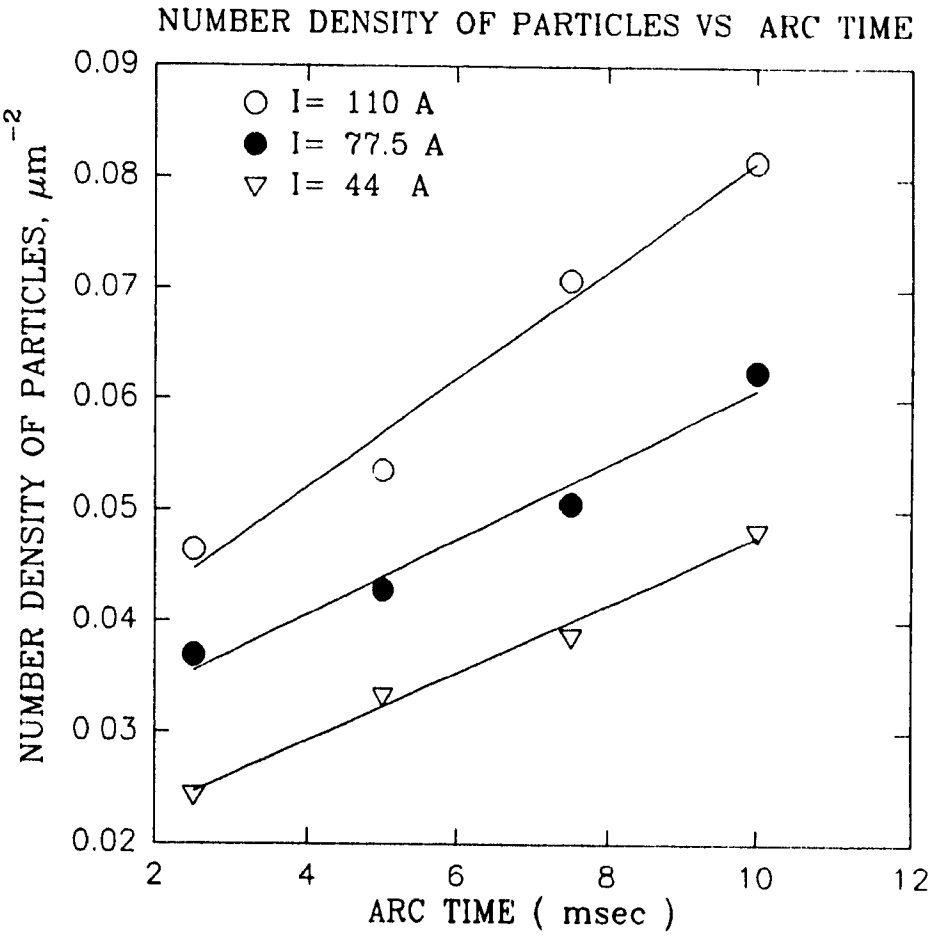

Figure (3-6) : Number density of particles as a function of the arc duration time, for I= 44 A, 77.5 A and 110 A, at D= 7.5 cm.

CATHODE SPOT TEMPERATURE

The temperature of the cathode spot should be an important factor affecting the size and the population of the particles emitted from the cathode spot. Temperature values shown in the following figures are calculated temperatures using the model described in section 2-2-2. Figures 3-7 and 3-8 show that the number and the size of the particles are directly proportional to the temperature of the cathode spot. Figure (3-7) represents the number density of particles counted using the image analyzer software described in section 2-2-4 as a function of cathode spot temperature calculated using the model in section 2-2-2. The actual temperature values at the cathode may not be that high, but because we only need to study the relative evolution of surface temperature for different arcing current I and arc time t, these values are acceptable. Since the temperature of the cathode spot depends on arc current I, arc voltage V and arc time t, the data in figure 3-7 have different values of I, V and t but constant number of coulombs (50 C). Figure 3-7 shows that the number of particles are directly proportional to the temperature of the cathode spot. This is due to the increase in the heat load which leads to an increase in the volume of the melted material from the cathode, which directly leads to an increase in the possibility of depositing more particles on the substrate.

Figures (3-8 a,b,c & d) represent the average size distribution of the particles deposited on the substrate as a function of the cathode spot temperature. The temperature values are calculated using the model described in section 2-2-2. The size distributions are measured using the image software analyzer connected to the SEM. For each figure the number of coulombs was constant and equal to 50 C.

From figure (3-8a), one can notice that at temperature around 700 K the average particle size is around 0.3 μm. At temperature around 1902 K as shown in figure (3-8b), the average particle size was increased to around 0.6 μm. As the temperature increases again to around 3059 K as shown in figure (3-8c), the average particle size was found to increase to around 0.8 μm. The largest average particle size found was around 1.2 μm at a temperature around 5538 K as shown in figure (3-8d).

These results show that the particle sizes increase with temperature. The above particle sizes are the average sizes found in each sample at constant number of coulombs (50 C) as described in section 2-2-4. In fact, Figure 3-8 shows that at any temperature level there is actually a range of particle sizes. The very small particles may be due to the dissociation that occurred on impact, as can be see in figure (3-9). The very large particles may be due to agglomeration that occurred on impact as shown in figure (3-10).

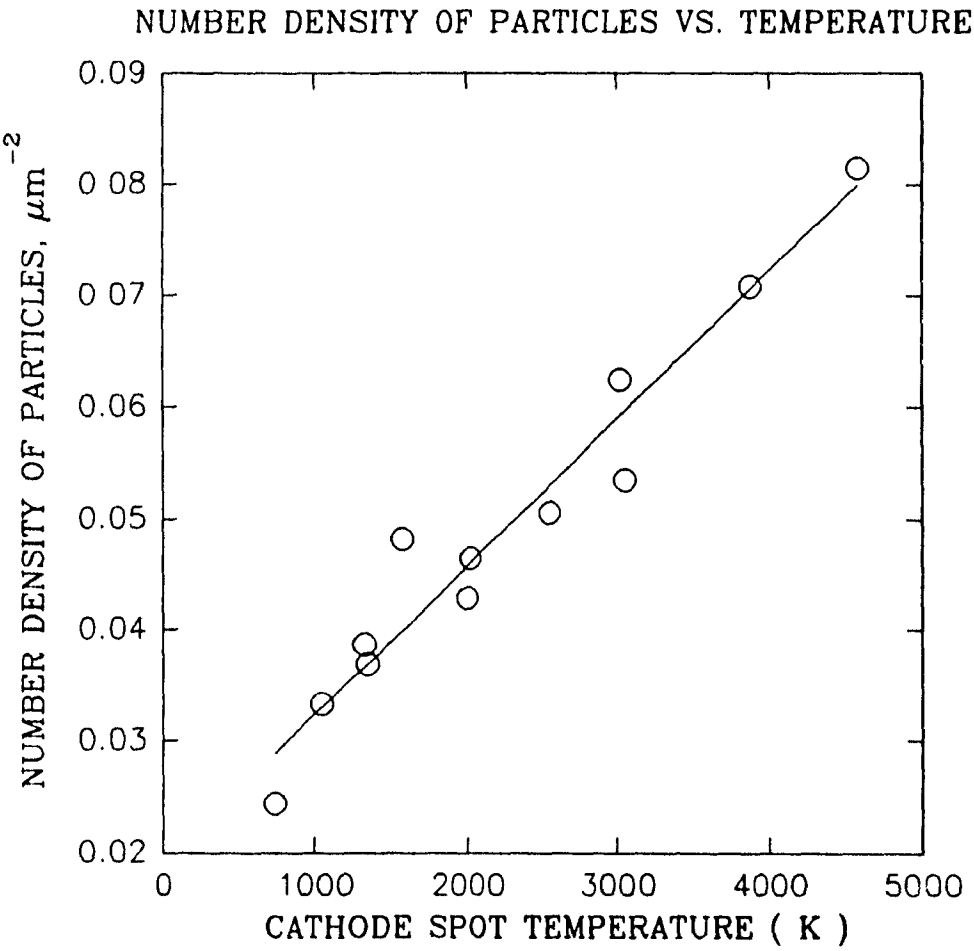

Figure (3-7) : Number density of particles as a function of cathode spot temperature, calculated from eqn. 2-5.

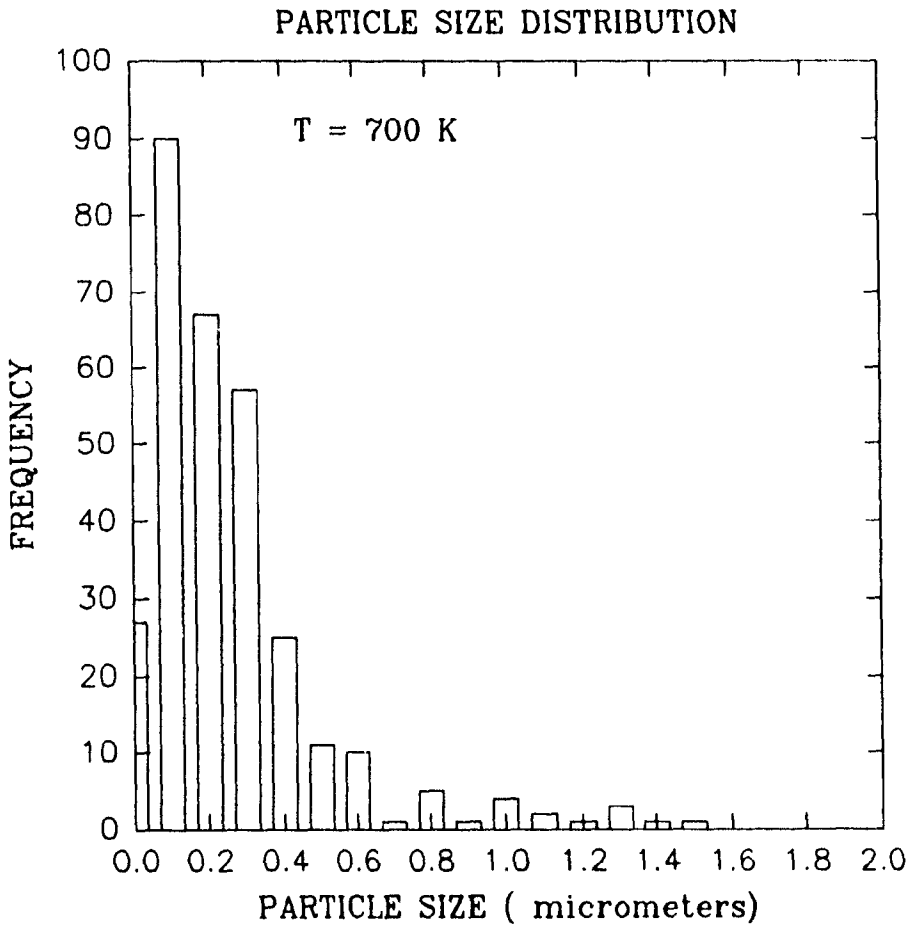

Figure (3-8a) Particle size distribution for cathode spot temperature around 700 K, calculated from eqn 2-5.

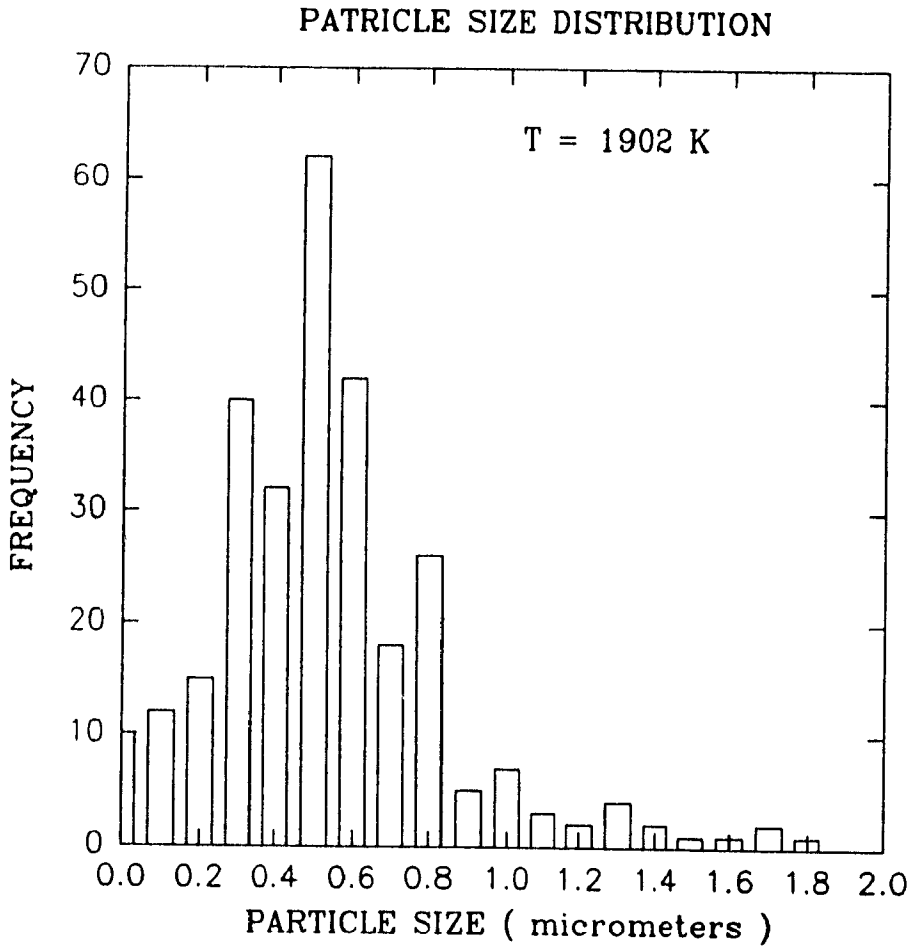

Figure (3-8b) : Particle size distribution for cathode spot temperature around 1902 K, calculated from eqn. 2-5.

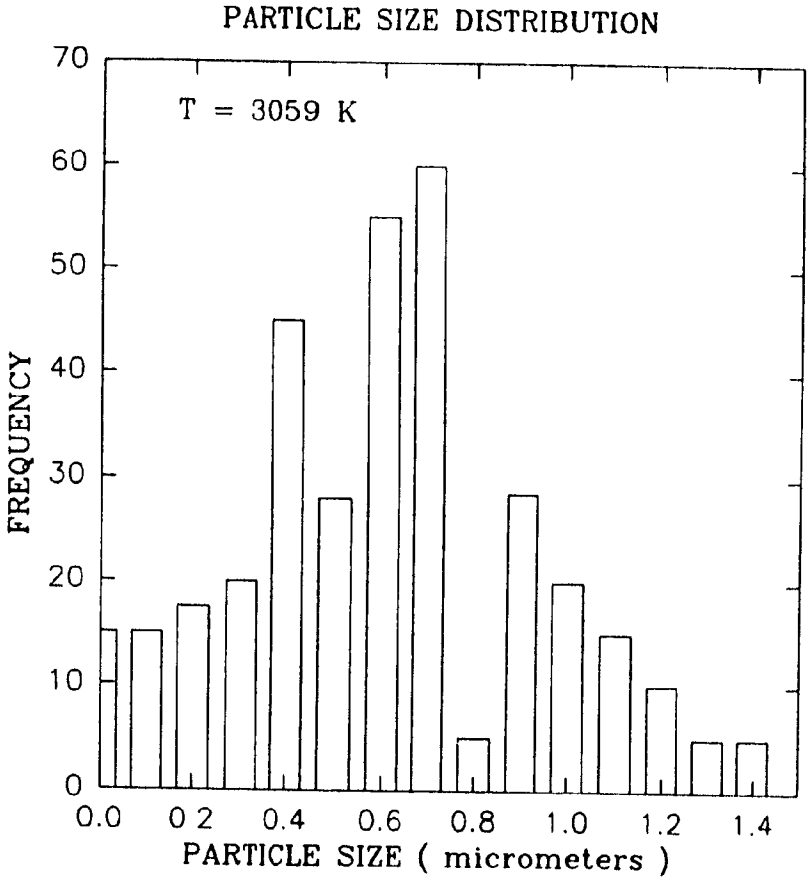

Figure (3-8c) : Particle size distribution for cathode spot temperature around 3059 K, calculated from eqn. 2-5.

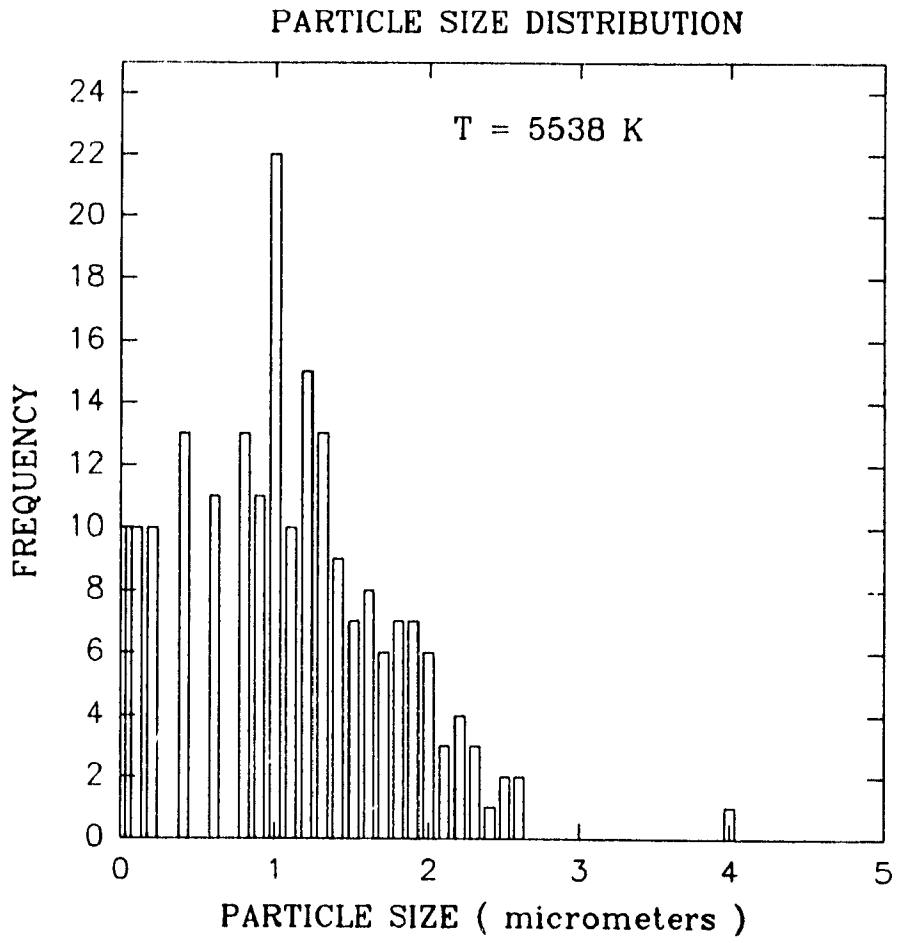

Figure (3-8d) : Particle size distribution for cathode spot temperature around 5538 K, calculated from eqn 2-5.

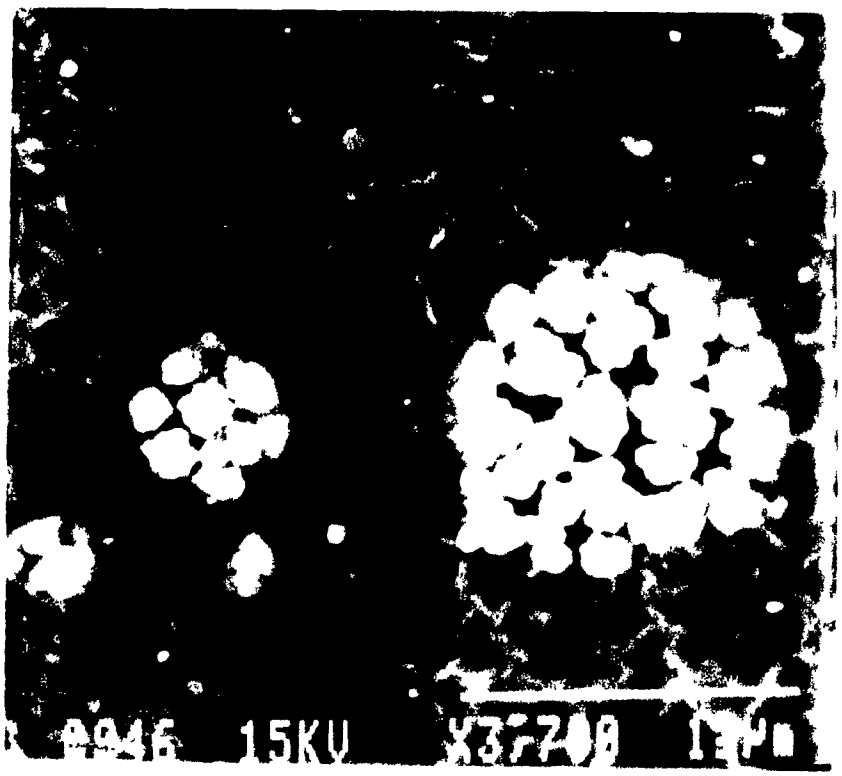

Figure (3-9) : SEM recording of a deposit on silicon in vacuum ($P=10^{-4}$ Pa), and t=5 ms, showing a large particle dissociation into several small particles on impact.

Figure (3-10) : SEM recording of a deposit on silicon in vacuum ($P=10^{-4}$ Pa), and complete discharge, showing small particles agglomerated to form large particles

3-1-2 : ORIGIN OF PARTICLES

Before the start of this experimental study, we considered several possibilities on the origin of the particles. We know from a large number of studies that the cathode is a source of particle emission. However, the anode may be another source because at certain deposition parameters, some anode spots are formed[31] which may emit micro-droplets. The possibility of the diamond growth from carbon ion bombardment at the substrate level is also not neglected at this point for the reasons described in section 1-2-2.

The particles emission from the anode depends on the arc current level. Low arc current permitted to avoid anode spot formation, which consequently avoided particles emission. In vacuum arcs, the anode fall voltage is usually low, since electron space charges at the anode surface are neutralized by the ion current incident on the anode from the cathode spots. Anode spot formation in vacuum occurs when the incident ion current is reduced, for example, by reducing the anode area or increasing the electrode separation [31]. In this study, the electrode geometry was designed to avoid anode spot formation. When anode spot occurred, this geometry provided the emitted particles of anode origin to be emitted in a direction opposite to the substrate. Depending on the operating parameters, some particles were in fact emitted by the anode. These, however, were not deposited on the substrate (see

figure 3-11), but were emitted in the opposite direction towards the cathode.

The origin of the particles that are deposited on the substrate seem clearly to be the cathode spots, as shown in figure (3-12) where the macro-particles emitted from the cathode, are travelling through the hole in the centre of the anode to the substrate.

For the possibility of substrate growth, we can say that none of the observed particles can reasonably have been grown on the substrate by the incoming ion flux. Such growth would require a high mobility of the carbon atoms at the surface and long deposition times compared to the short pulses used. In flight nucleation seems also impossible because of the very long mean free paths of collision between the ions (typically in the order of the cathode to substrate distance). However, ideal conditions for diamond-like film growth were not the object of this study and we can not exclude the growth of the cauliflower type particles in such circumstances.

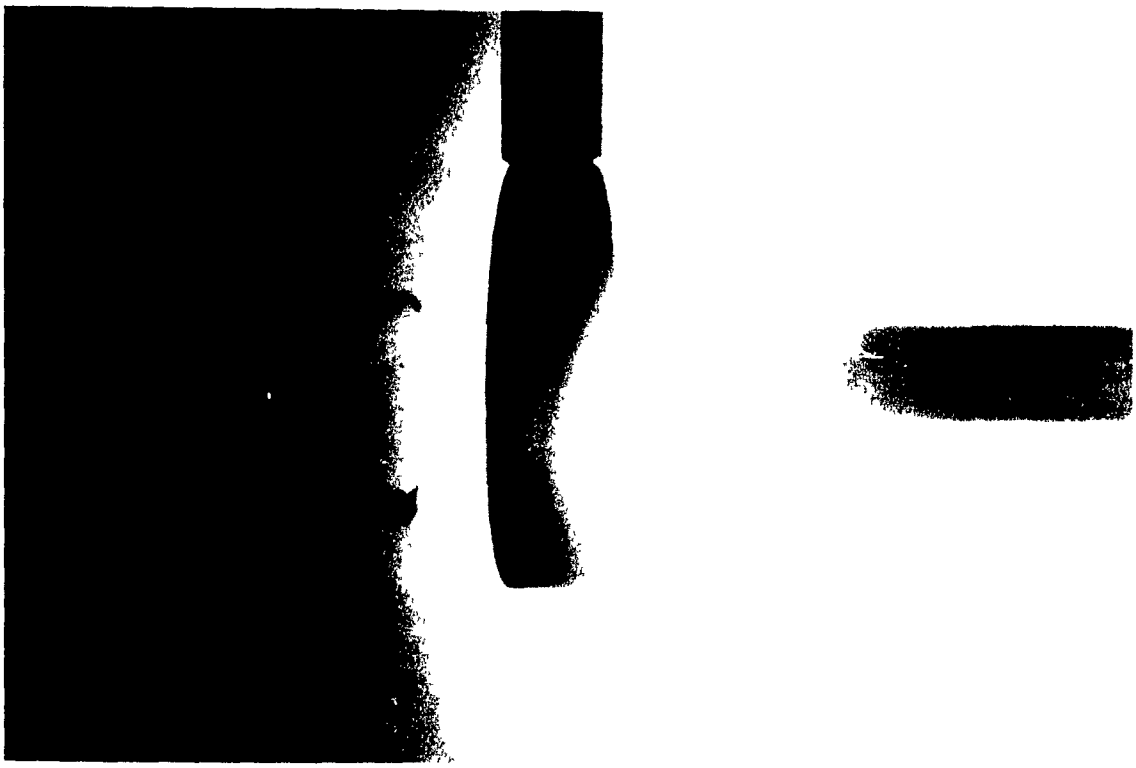

Figure (3-11) : A photograph shows the emission of the particles from the anode,and reflected far from the substrate.

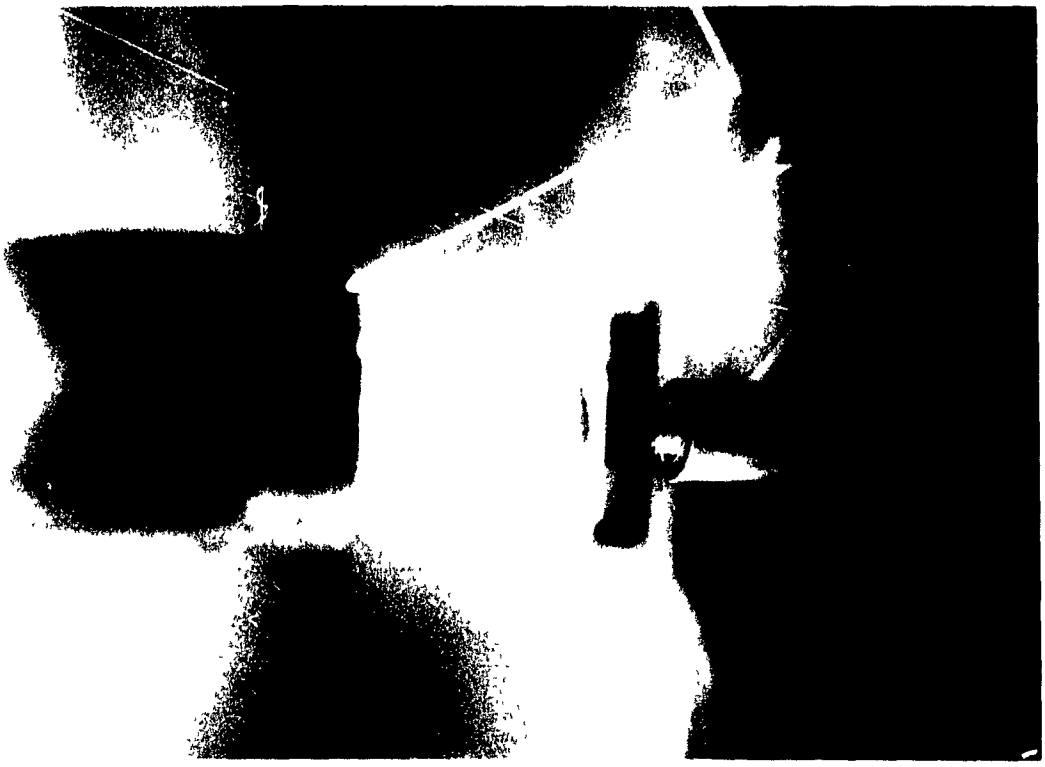

Figure (3-12) : A photograph shows the emission of the particles from the cathode to the substrate.

3-1-3 : PARTICLES STRUCTURE

The first diagnostic technique used in this work to study the crystal structure is the X-Ray Diffraction technique. This technique was unsuccessful in the present study because it needs milligrams of the deposited material on the substrate and this was not possible for our samples. The second diagnostic technique is Raman Spectroscopy, which is available in the Chemistry Department at McGill University. This technique was also unsuccessful because it could not resolve the small micron-size particles. The most useful technique for the analysis of the particles and background structures in this study was the Auger Electron Spectroscopy (AES), that is available in Hydro Quebec (IREQ). This technique was able to analyze very thin surface layers and very small particles sizes with very high resolution. Clear interpretation of the results for carbon films constitutes, however, a major difficulty of AES.

Figure (3-13) shows typical AES spectra for Diamond, Graphite, & Amorphous carbon films. This figure will be used as a reference for comparison purposes with our own AES profiles.

Figure (3-14) shows a spectrum of a deposit made on silicon wafer in vacuum ($P = 10^{-4}$ torr) with arc time (t = 14 ms), and distance between the cathode and the substrate (D = 7.5 cm). This spectrum shows the AES carbon structure of one particle in the deposited carbon film. As one can see, the spectrum shows the typical AES behaviour of graphite. A spectrum of another particle in the same

layer is shown in figure (3-15), showing a graphite and amorphous mixture structure. The spectrum in figure (3-16) is for the same sample, but it shows the structure of the background film close to the particle. Interpretation of this spectrum is more difficult. The confusion may come from the large number of particles that are found in this sample, i.e., the background that was chosen for analysis had some very small particles which affect the structure. This becomes clear by taking a look at figure (3-17) which shows a spectrum for another sample with the same operating conditions except the distance D = 45 cm. This sample shows a smaller density of particles compared to the previous one. This spectrum seems to show some diamond characteristics for the background although this interpretation may still be very subjective. Figures(3-18) & (3-19) show the morphology for both samples by using Electron Scanning Microscopy (SEM).

The spectrum in figure (3-20) for a deposit on silicon wafer in vacuum (P= 10^{-4} torr), with arc time (t=0.5 ms) and D=7.5 cm, shows the structure of a particle in this carbon film. We see again a structure showing the main characteristics of graphite by comparing this spectrum with the typical one shown in figure (3-13).

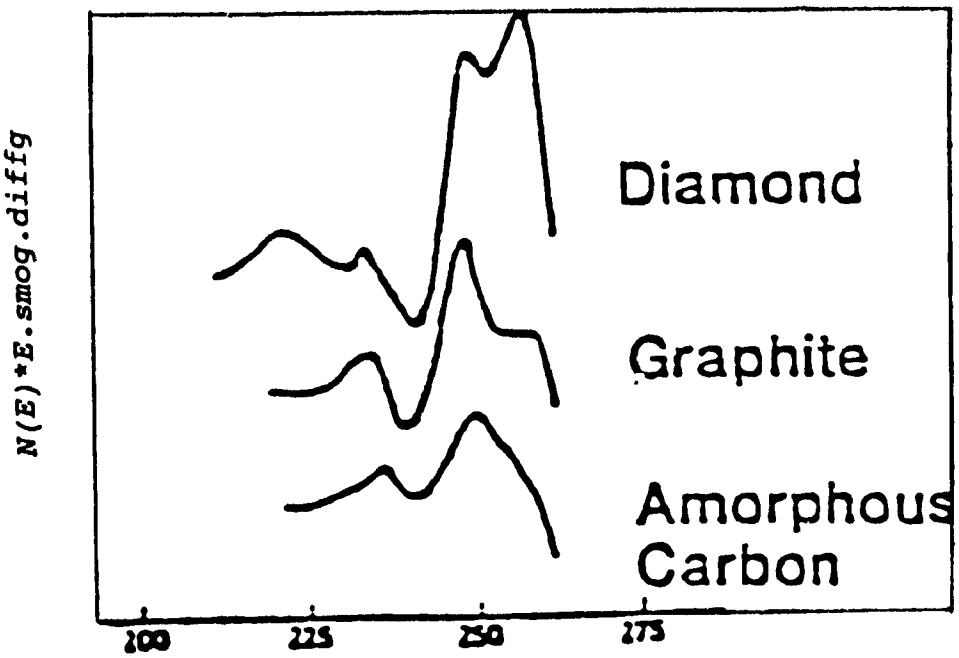

Figure (3-13) : Typical AES spectra for diamond, Graphite and amorphous carbon films[32].

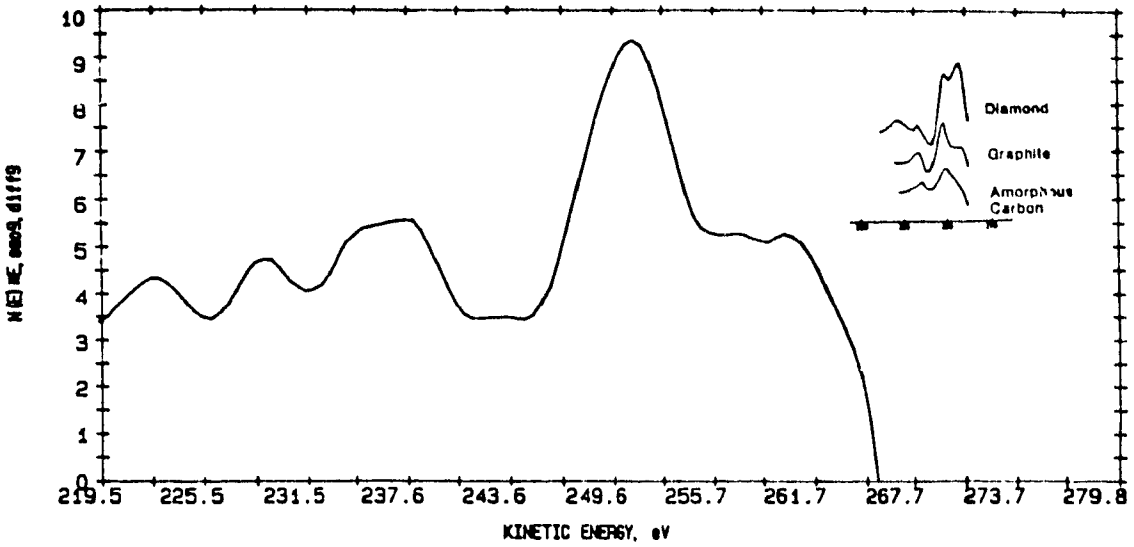

Figure (3-14) : AES spectrum for a particle deposited on silicon in vacuum P = 10^{-4} torr, t= 14 ms, D= 7.5 cm and Q=100 C.

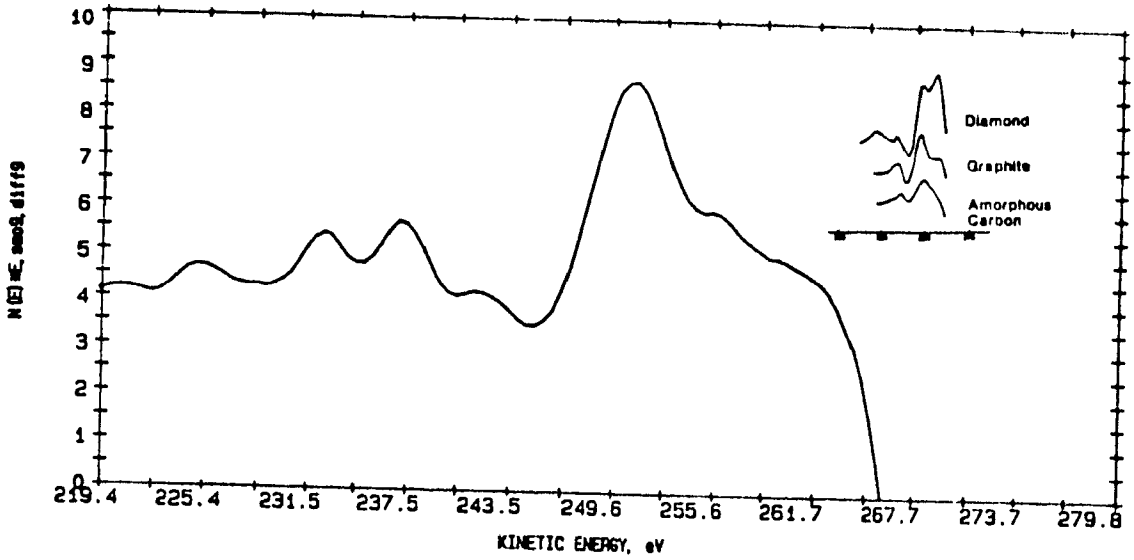

Figure (3-15) : AES spectrum for another particle on the same sample shown in figure (3-14).

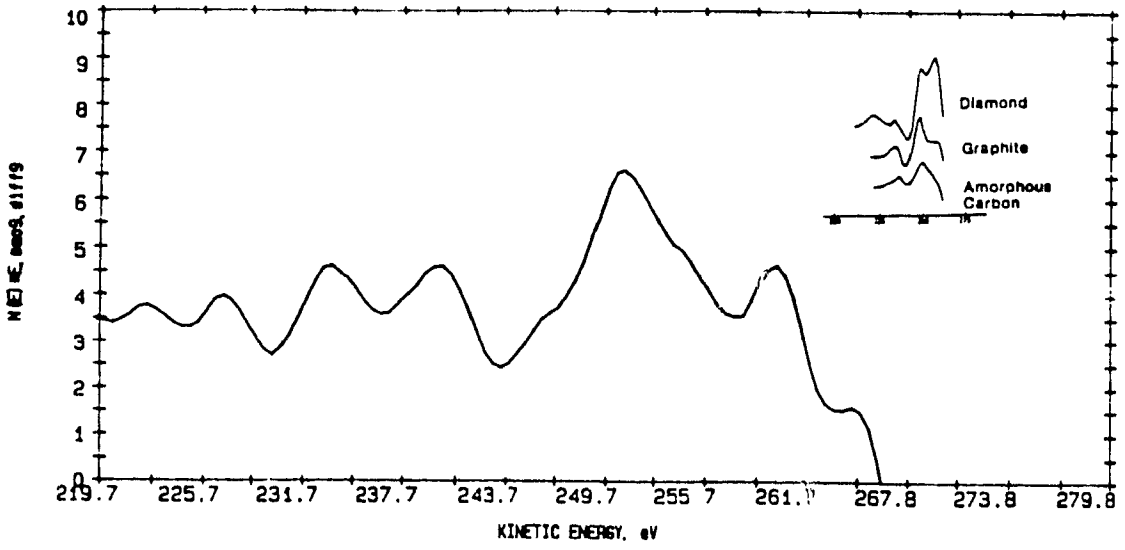

Figure (3-16) : AES spectrum for the background deposited on silicon in vacuum P= 10^{-4} torr,t= 14 ms, D= 7.5 cm & Q=100 C.

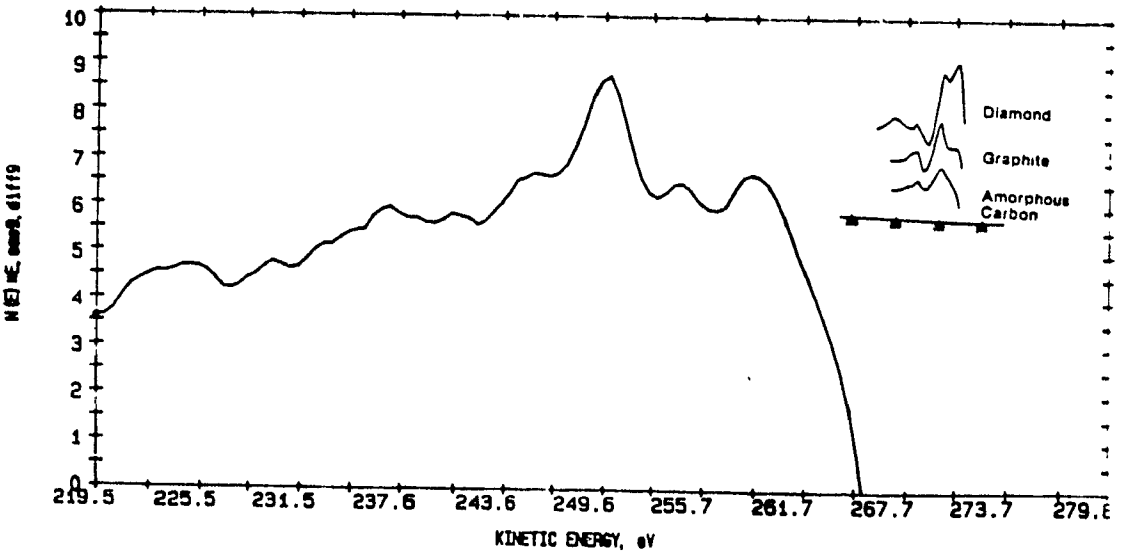

Figure (3-17) : AES spectrum for the background deposited on silicon in vacuum P= 10^{-4} torr, t= 14 ms, D=45 cm,& Q=100 C.

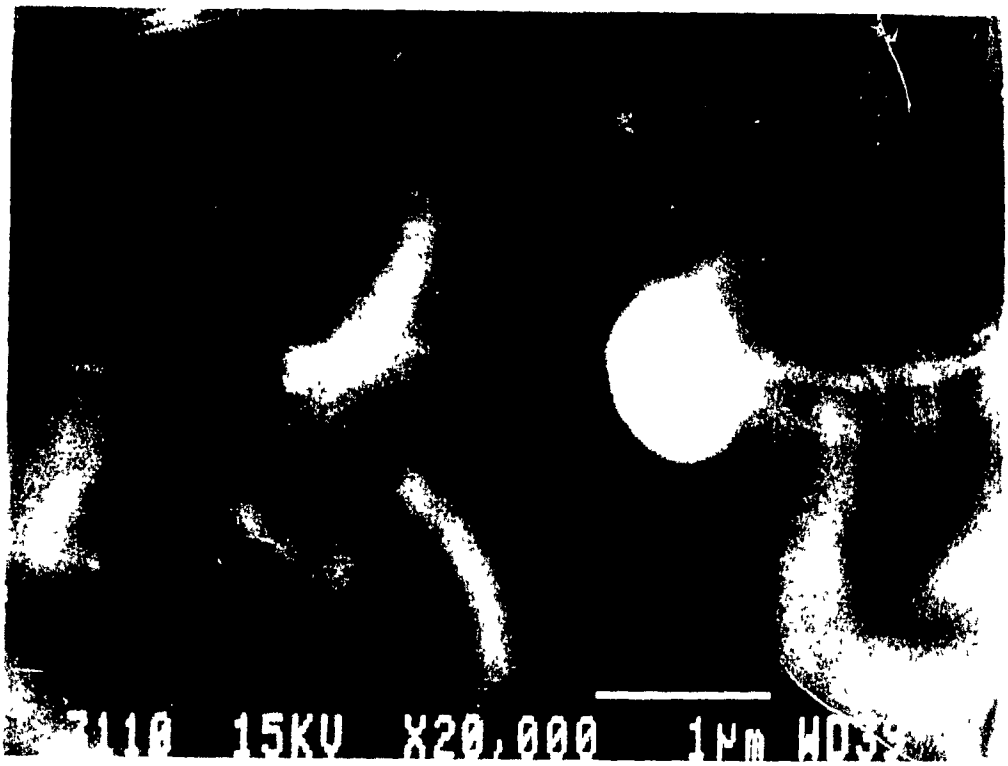

Figure (3-18) : SEM recording shows the morphology of a particle deposited on the silicon in vacuum P= 10^{-4} torr, t= 14 ms, D=45 cm, and Q= 100 C.

Figure (3-19) : SEM recording shows the morphology of the particles deposited on silicon in vacuum P=10^{-4} torr, t= 14 ms, D=7.5 cm, and Q= 100 C.

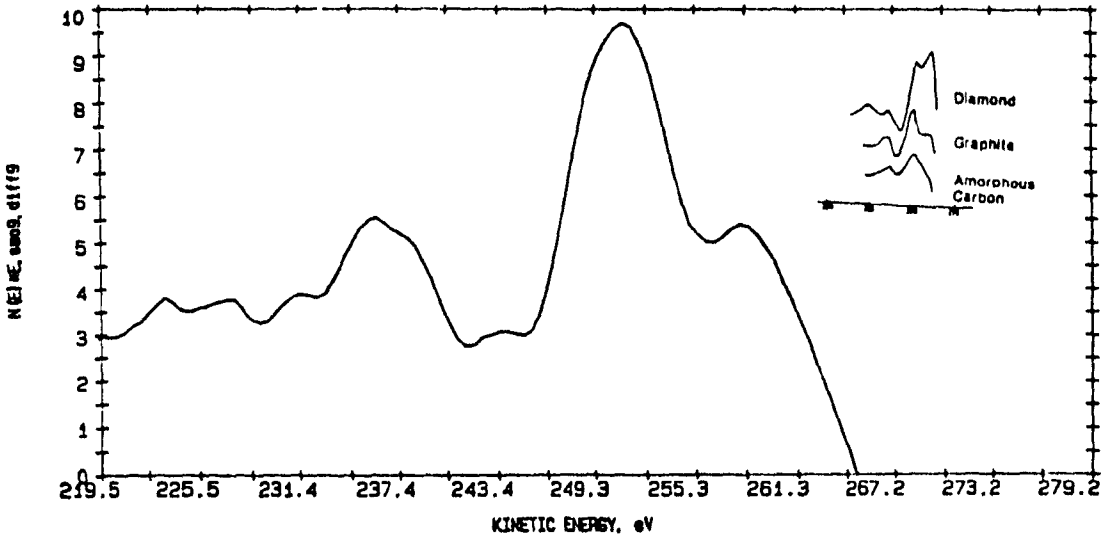

Figure (3-20) : AES spectrum for a particle deposited on silicon in vacuum P= 10^{-4} torr, t= 0.5 ms, D= 7.5 cm & Q=10 C.

DISCUSSION

PARTICLE AND FILM STRUCTURE

For both the particles and the deposited carbon film, the morphology were analyzed by using SEM, and the structure by using AES.

The structure of all the particles was found as a graphite structure, in spite of the change in the operating conditions. The claim by some researchers of the international community (unpublished data) that particles emitted by vacuum arc plasmas on graphite cathodes had microcrystalline diamond structure was not verified in this work. The structure of the background (i.e., the deposited carbon film) seem to be mainly graphite with some diamond characteristics, as shown in Figure (3-17).

The focus of this study was aimed at the generation mechanism of particles in the films, and not to obtain good diamond-like films. AES however show some evidence of the amorphous structure of the film. A better control of operating conditions could lead to diamond-like films.

The ion energy for carbon arc is approximately 30 eV for C^{+} and 20 eV for C^{++} [13]. Studies on ion beam generated diamond-like films showed the need of carbon ion energy is usually around 100 eV [33]. Vacuum arc generated carbon ions have maximum energy around 30 eV (see figure 1-7). We can thus assume that a negative substrate bias may be needed to produce good diamond-like films.

One must keep in mind however that vacuum arc deposited TiN films can be done at much lower substrate bias than needed for sputtering processes [15]. The reason for this being attributed to the large degree of ionization in the vacuum arc process compared to the sputtering techniques. The same effect may possibly apply in the case of diamond-like.

PARTICLES ORIGIN

The possible origins that I mentioned in section (3-1-2) are the emission from the anode, from the cathode or formation at the substrate level as a result of the bombardment of the substrate by the high energized atoms emitted from the cathode. The origin of the particles in this study was definitely the cathode. The particles are found in all the samples, at any deposition parameter values and clearly show signs of impact assimilated to a projection process. We thus neglect here the possibility of the formation of the droplets at the substrate level. As shown for example in figure (3-12),the cathode spot is clearly the origin of the micro-droplets and the possibility of cauliflower type diamond particle growth at the substrate is most likely not to happen. This conclusion should be tested again on a diamond-like vacuum arc deposition system eliminating particles of cathode origin.

ARC CURRENT LEVEL

The size and the number of the micro-particles are found

directly proportional to the intensity of the arc current. The maximum current per spot is limited, and depends on the cathode material (i.e., for carbon 200 A/spot). In this work, the arc current was always below 200 A, which means no increase should be expected in the number of the spots. The increase in the arc current at constant number of coulombs may lead to an increase in the spot size and the spot temperature. This increases the volume of the material melted and emitted from the cathode as a result of the strong plasma pressure above the spot and the strong explosive nature of the cathode spot life. In the case of graphite cathodes, the intense thermal shock proportional to the arc current level in the spot area may also induce cracking of the porous graphite structure. Although most particles observed had a melted-like shape, some larger particles having irregular shapes may have been emitted through this process.

CATHODE SPOT TEMPERATURE

The size and population of micro-droplets are found directly proportional to the calculated temperature of the cathode spot. Melting effects due to the thermal load are thus the main source of emitted particles. A given spot temperature was induced in this study by varying either the arc current or the arc duration time.

The question that may arise here is: can particles be eliminated at low temperature values ?

A given number of coulombs will always be needed to produce

the ions necessary for film growth. In order to decrease the temperature at constant number of coulombs, we need to decrease the arc current and/or the arc residence time while adjusting the number of arcs in a pulse system. Both have limiting values, and below these values the arc becomes very unstable and will extinguish. The other possibility to decrease the temperature of the cathode spot is by moving the arc magnetically, decreasing the residence time of the arc at a given location on the cathode. This technique may help to reduce the number of emitted particles to a very small value. Such a technique constitutes a next step in the future leading to a continuous deposition system. The porosity of the cathode may always affect the particle emissions to a certain degree. More porosity leads to an increase of the temperature gradients around the cathode spot, which causes mechanical removal and consequently an increase in the number of the emitted particles. Consequently, low porosity graphite cathodes should always be used.

The smallest residence times used in this project was 2.5 ms (except one run at 0.5 ms and 10 C), although residence times around 10 μs can be attained with our experimental set up. This can be used as an upper limit in the design of a continuous system to evaluate the arc velocity and magnetic field strength needed. This residence time spread over a distance similar to the size of our cathode leads to a few meters/second velocity.

Magnetic stirring of vacuum arcs on metallic electrodes is

commonly done in our lab and industrially. The same technique, however, seems to cause problems of arc instability and anchoring effects on graphite cathodes. A study of the magnetic field strength to drive such an arc velocity is needed.

Finally, all data suggest a decrease in cathode temperature will decrease the number of emitted particles. We can hence conclude that a good cathode cooling to very low temperature may greatly help to solve this problem.

DISTANCE BETWEEN THE CATHODE AND THE SUBSTRATE

At constant number of charges passing through the cathode, the size and concentration of the micro-droplets are inversely proportional to the distance between the cathode and the substrate. This follows the solid angle distribution as shown in figure (3-5), where the particle density per solid angle were approximately constant. This simply means that the particles travel along straight-lines.

PARTICLE SIZE DISTRIBUTION

The particles size distribution results are interesting and important. The mean particles sizes are found to be directly proportional to the cathode spot temperature. It can thus be correlated to the melting action at the cathode spot producing a pool of melted material having a volume proportional to the thermal load. Larger melted pool volumes would produce larger particles.

Integrating the distributions of Figures 3-8 a,b,c & d leads to values of the total particle volume for a given substrate area of 1681 μm^2. The volumes obtained when increasing temperature were $2.631*10^5$ μm^3 at 700 K, $1.557*10^6$ μm^3 at 1902 K, $4.567*10^6$ μm^3 at 3059 K and $6.036*10^6$ μm^3 at 5538 K. These values correspond to masses of 0.60513 μg, 3.5811 μg, 10.5041 μg and 13.8828 μg respectively, or mass densities of $3.6x10^{-4}$ $\mu g/\mu m^2$, $2.13x10^{-3}$ $\mu g/\mu m^2$, $6.25x10^{-3}$ $\mu g/\mu m^2$, $8.26x10^{-3}$ $\mu g/\mu m^2$ respectively.

The larger agglomerated particles would be produced when enough large size and slow in flight cooling time particles can reach the substrate. The importance of the large size tail of the distribution for the high temperature cases (see for example figure 3-8d) compared to the lower temperature cases is a good indication of this phenomenon. The small particle size portion of the distribution is also more important in the high temperature situation. This may reflect the poorer mechanical integrity of the large emitted particles that break upon impact forming a larger number of small size particles.

CONCLUSION

The main objective of the present work is the studying of the generation mechanisms and characteristics of the droplets that are formed in the carbon films produced by VAD techniques. A limiting factors in applying the VAD method relates to the deposition of micro-particles. For many applications, the presence of any micro-particles is unacceptable. Much progress has been made during recent years in producing films that, while not completely free of particles, are a significant improvement on the film that were produced at earlier stages.

As a conclusion of the present study, the micro-droplets formed in the carbon film is graphite. These droplets have sizes ranged from 0.3 μm to 2 μm, and originate from the cathode. The droplet production is mainly due to the heating effect which can be controlled by changing arc current level and/or arc duration time. The number and size of these micro-droplets can be decreased by lowering the temperature of the cathode spot and/or increasing the distance between cathode and substrate.

In our experimental conditions, no lower limit to the emission of droplets was found, leaving room for much improvement.

REFERENCES :

1. *S.Aisenberg and R.Chabot, "Ion beam deposition of thin films of diamond-like carbon ", J.Appl.Phys., Vol. 42, NO.7, pp. 2953-2958, 1971.*
2. *E.G.Spencer, P.H.Schmidt, D.H.Joy, F.J.Sansalone, "Ion beam deposition poly crystalline diamond-like films " Appl. Phys. Lett., Vol. 29, No. 2, PP. 118-120, July 1976.*
3. *J.H.Freeman, W.Temple. G.A.Gard, " The epitaxial synthesis of diamond by the deposition of low energy carbon ions ", Vacuum, Vol. 34, No. 1-2, PP. 305-314, 1984.*
4. *See review in Y.Lifshitz, S.R.Kasi, J.W.Rabalais, " mass selected ion beam deposition : a tool for parametric growth studies, process development and fabrication of diamond-like films", Adv.Mater. & Manuf. Processes, Vol.3, No. 2, PP. 157-194, 1988.*
5. *L.P.Andersson, "A review of recent work on hard i-C films", Thin Solid Films, 88, PP. 193-200, 1981.*
6. *C.W.Kimblin, " Cathode spot erosion phenomena in the transition from vacuum to atmospheric pressure arcs ", J.Appl.Phys., 45, 12, 1974, PP. 5235-5244.*
7. *P.C.Johnson, " The Cathodic Arc Plasma Deposition of Thin Films", Physics of Thin Films, Vol. 14, pp. 129-199, 1989.*
8. *Raymond L.Boxman, " Principles and applications of vacuum arc coatings", IEEE Transaction on Plasma Science, Vol.17,*

No.5, October 1989.

9. A.I.Maslov, G.K.Dmitriev, Y.D.Chistyakov, " Pulsed Carbon-Plasma Source For Production Processes", Prib. Tech. Eksp., Vol. 3, 1985, PP. 146-149.

10. M.Douyon de Azevodo, J.-L.Meunier, "Ion flux intensity measurements on carbon spot plasma interaction with low pressure hydrogen ," in Proc. 14th. Int. Symp. on Disch.and Elect. Ins. in vac., Santa Fe,N.M, Sept. 17-20, 1990.

11. J.M.Lafferty, "Vacuum Arc-Theory and Application", pp.120-168, John Wiley & Sons, Toronto 1980.

12. E.O.Johnson and L.Matter, "A Floating Double Probe Methode for Measurements in Gas Discharge", Phys.Rev. 80,50 (1950).

13. W.D.Davis and H.C.Miller, " Analysis of the electrode products emitted by DC arcs in a vacuum ambient", J.Appl. Phys. 40, 2212 (1969).

14. M.Douyon de Azevedo, J.-L.Meunier, "Vacuum arc deposition of carbon thin films in a low pressure of hydrogen:, IEEE Trans. on Plasma Sci. Vol. 19, No. 5, October 1991.

15. T.Utsumi and J.H.English, "Study of electrode products emitted by vacuum arcs in form of molten metal particles",J.Appl.Phys.46,126-131 (1975).

16. D.T.Tuma, C.L.Chen and D.K.Davies, "Erosion products from the cathode spot region of a copper vacuum arc", j.Appl.Phys.49(7),1978.

17. J.E.Daalder, " Components of cathode erosion in vacuum arcs", J-Phys.D:Appl.Phys. 9, 2379-2395 (1976).

18. J.E.Daalder " Cathode spots and vacuum arcs ", Physica 104C, pp. 91-106, 1981.

19. I.I.Aksenov et al.Sov.J.Plasma Phys.4(4),425-428 (1978).

20. I.I.Aksenov,V.G.Padalka,N.S.Repalov and V.M.Khoroshikh, Sov. J.Plasma Phys. 6(2), 173-176 (1980).

21. Yoshikatsu Namba, Jin Wei, Toshio Mohri, and E.A.Heidarpour, "Large grain size thin films of carbon with diamond structure", J.Appl. Phys. (184) (1988).

22. J.-L.Meunier, M.G.Drouet,"Experimental study of the effect of gas pressure on arc cathode erosion and redeposition in He, Ar and SF_6 from vacuum to atmospheric pressure", IEEE Trans. Plasma Sci., 15,5,1987,pp. 515-519.

23. S.Matsumoto, Y.Sato, M.Tsutsumi, N.Setaka, "Growth of diamond particles from methane-hydrogen gas", J.Mater. Sci. Vol. 17,pp. 3106-3112, 1982.

24. D.S.Knight, W.B.White,"Characterization of diamond films by Raman spectroscopy", J.Matter. Res. Vol. 4, No. 2, pp. 385-393, May/April 1989.

25. S.Aisenberg and R.W.Chabot, " Ion-beam deposition of thin films of diamondlike carbon", J.Appl.Phys., 42 (1971) 2953.

26. Ludvik Martinu, " Amorphous carbon films", High Energy Density Technologies in Materials Science, 77-87, 1990

27. J.-L.Meunier,"Pressure limit for the vacuum arc deposition technique," IEEE Trans. on Plasma Sci. Vol. 18, No. 6,

Oct. 1990.

28. A.I.Brown, S.M.Marco,"Introduction to heat transfer", McGrow-Hill, pp. 258-265, 1985.

29. V.I.Rakhoviskii, IEEE Trans. on plasmas science PS-4(2), 81-102 (1976).

30. C.W.Kimblin,"Erosion and ionization in the cathode spot regions of vacuum arcs," J.Appl.Phys., Vol. 44, No. 7, July 1973.

31. M.G.Drouet, "Anode Spots and Cathodic Plasma Flow in a Vacuum Arcs," J.Phys.D:Appl.Phys.,Vol.14, pp. L211-214, 1981.

32. B.E.Williams, J.T.Glass, Materials Research Society, 60 (1988).

33. J.C.Angus, P.Koidl, S.Domitz, "Plasma Deposited Thin Films", J.Mart, F.Jansen eds. chapt. 4,CRC press 89-127, 1986.